

# Five new pseudocryptic land planarian species of *Cratera* (Platyhelminthes: Tricladida) unveiled through integrative taxonomy (#48478)

1

First submission

## Guidance from your Editor

Please submit by **30 May 2020** for the benefit of the authors (and your \$200 publishing discount) .



### Structure and Criteria

Please read the 'Structure and Criteria' page for general guidance.



### Custom checks

Make sure you include the custom checks shown below, in your review.



### Author notes

Have you read the author notes on the [guidance page](#)?



### Raw data check

Review the raw data.



### Image check

Check that figures and images have not been inappropriately manipulated.

Privacy reminder: If uploading an annotated PDF, remove identifiable information to remain anonymous.

## Files

Download and review all files from the [materials page](#).

17 Figure file(s)

2 Table file(s)

## ! Custom checks

### DNA data checks

- ! Have you checked the authors [data deposition statement](#)?
- ! Can you access the deposited data?
- ! Has the data been deposited correctly?
- ! Is the deposition information noted in the manuscript?

### Field study

- ! Have you checked the authors [field study permits](#)?
- ! Are the field study permits appropriate?

### New species checks

- ! Have you checked our [new species policies](#)?



Do you agree that it is a new species?



Is it correctly described e.g. meets ICZN standard?


For assistance email [peer.review@peerj.com](mailto:peer.review@peerj.com)



## Structure your review

The review form is divided into 5 sections. Please consider these when composing your review:

1. BASIC REPORTING
2. EXPERIMENTAL DESIGN
3. VALIDITY OF THE FINDINGS
4. General comments
5. Confidential notes to the editor






 You can also annotate this PDF and upload it as part of your review

When ready [submit online](#).





## Editorial Criteria

Use these criteria points to structure your review. The full detailed editorial criteria is on your [guidance page](#).





### BASIC REPORTING

-  Clear, unambiguous, professional English language used throughout.
-  Intro & background to show context. Literature well referenced & relevant.
-  Structure conforms to [PeerJ standards](#), discipline norm, or improved for clarity.
-  Figures are relevant, high quality, well labelled & described.
-  Raw data supplied (see [PeerJ policy](#)).

### EXPERIMENTAL DESIGN

-  Original primary research within [Scope of the journal](#).
-  Research question well defined, relevant & meaningful. It is stated how the research fills an identified knowledge gap.
-  Rigorous investigation performed to a high technical & ethical standard.
-  Methods described with sufficient detail & information to replicate.

### VALIDITY OF THE FINDINGS

-  Impact and novelty not assessed. Negative/inconclusive results accepted. *Meaningful* replication encouraged where rationale & benefit to literature is clearly stated.
-  All underlying data have been provided; they are robust, statistically sound, & controlled.
-  Speculation is welcome, but should be identified as such.
-  Conclusions are well stated, linked to original research question & limited to supporting results.

# Standout reviewing tips

3



The best reviewers use these techniques

## Tip

**Support criticisms with evidence from the text or from other sources**

## Example

*Smith et al (J of Methodology, 2005, V3, pp 123) have shown that the analysis you use in Lines 241-250 is not the most appropriate for this situation. Please explain why you used this method.*

**Give specific suggestions on how to improve the manuscript**

*Your introduction needs more detail. I suggest that you improve the description at lines 57- 86 to provide more justification for your study (specifically, you should expand upon the knowledge gap being filled).*

**Comment on language and grammar issues**

*The English language should be improved to ensure that an international audience can clearly understand your text. Some examples where the language could be improved include lines 23, 77, 121, 128 – the current phrasing makes comprehension difficult.*

**Organize by importance of the issues, and number your points**

1. Your most important issue
2. The next most important item
3. ...
4. The least important points

**Please provide constructive criticism, and avoid personal opinions**

*I thank you for providing the raw data, however your supplemental files need more descriptive metadata identifiers to be useful to future readers. Although your results are compelling, the data analysis should be improved in the following ways: AA, BB, CC*

**Comment on strengths (as well as weaknesses) of the manuscript**

*I commend the authors for their extensive data set, compiled over many years of detailed fieldwork. In addition, the manuscript is clearly written in professional, unambiguous language. If there is a weakness, it is in the statistical analysis (as I have noted above) which should be improved upon before Acceptance.*

# Five new pseudocryptic land planarian species of *Cratera* (Platyhelminthes: Tricladida) unveiled through integrative taxonomy

Ana Paula G Araujo<sup>1,2</sup>, Fernando Carbayo<sup>2,3</sup>, Marta Riutort<sup>4</sup>, Marta Álvarez-Presas<sup>Corresp. 4</sup>

<sup>1</sup> Museu de Zoologia, Universidade de São Paulo, São Paulo, Brazil

<sup>2</sup> Laboratório de Ecologia e Evolução, Escola de Artes, Ciências e Humanidades, Universidade de São Paulo, São Paulo, Brazil

<sup>3</sup> Departamento de Zoologia, Instituto de Biociências, Universidade de São Paulo, São Paulo, Brazil

<sup>4</sup> Departament de Genètica, Microbiologia i Estadística, Facultat de Biologia and Institut de Recerca de la Biodiversitat (IRBio), Universitat de Barcelona, Barcelona, Spain

Corresponding Author: Marta Álvarez-Presas  
Email address: onaalvarez@ub.edu

**Background.** *Cratera* is a genus of land planarians endemic to the Atlantic forest. The species of this genus are distinguished from each other by a series of external and internal characters, nonetheless they represent a challenging taxonomic issue due to the extreme likeness of the species analysed on the present work. To resolve these difficulties, we have performed morphological analyses and used five nuclear and mitochondrial genes in an integrative taxonomic study.

**Methods.** To unveil eventual cryptic species, we applied a molecular species delimitation approach based on molecular discovery methods, followed by a validation method. The putative species so delimited were then validated on the basis of the existence of morphological features that differentiated them.

**Results.** By doing so, we have discovered and described four new species, namely *Cratera piguaiassu*, *C. piguaiatui*, *C. piguaiaboja*, and *C. imbiru*. A fifth new species, *C. paraitinga* was not highly supported by molecular evidence but was described because its morphological attributes were unique. As a result, we find again the existence of high similarity among terrestrial planarians as has already been described in other genera. The high number of young species poorly differentiated might be explained by the recent history of the area.

# Five new pseudocryptic land planarian species of *Cratera* (Platyhelminthes: Tricladida) unveiled through integrative taxonomy

Ana Paula G. Araujo<sup>1,3</sup>, Fernando Carbayo<sup>2,3</sup>, Marta Riutort<sup>4</sup>, Marta Álvarez-Presas<sup>4</sup>

<sup>1</sup> Museu de Zoologia da Universidade de São Paulo, Ipiranga, São Paulo, SP, Brazil

<sup>2</sup> Departamento de Zoologia, Instituto de Biociências, Universidade de São Paulo, São Paulo, SP, Brazil

<sup>3</sup> Laboratório de Ecologia e Evolução, Escola de Artes, Ciências e Humanidades, Universidade de São Paulo, São Paulo, SP, Brazil

<sup>4</sup> Departament de Genètica, Microbiologia i Estadística, Facultat de Biologia and Institut de Recerca de la Biodiversitat (IRBio), Universitat de Barcelona, Barcelona, Catalonia, Spain

Corresponding Author:

Marta Álvarez-Presas<sup>4</sup>

Av. Diagonal 645, Barcelona, Catalonia, 08028, Spain

Email address: coseseries@gmail.com

## Abstract

**Background.** *Cratera* is a genus of land planarians endemic to the Atlantic forest. The species of this genus are distinguished from each other by a series of external and internal characters, nonetheless they represent a challenging taxonomic issue due to the extreme likeness of the species analysed on the present work. To resolve these difficulties, we have performed morphological analyses and used five nuclear and mitochondrial genes in an integrative taxonomic study.

**Methods.** To unveil ~~eventual~~ cryptic species, we applied a molecular species delimitation approach based on molecular discovery methods, followed by a validation method. The putative species so delimited were then validated on the basis of ~~the existence of~~ morphological features ~~that differentiated them.~~

**Results.** ~~By doing so, we have~~ discovered and described four new species, namely *Cratera piguaiassu*, *C. piguaiatui*, *C. piguaiaboja*, and *C. imbiru*. A fifth new species, *C. paraitinga* was

not highly supported by molecular evidence but was described because its morphological attributes were unique. As a result, we find again the existence of high similarity among terrestrial planarians as has already been described in other genera. The high number of young species poorly differentiated might be explained by the recent history of the area.

## Introduction

Land planarians (Platyhelminthes: Tricladida: Geoplanidae) are mostly soil inhabitants of forested areas. There are over 900 known species (Sluys, 2016), 332 of them belonging to Geoplaninae (<http://planarias.each.usp.br>; accessed in 18. March 2020), an exclusively Neotropical subfamily. Anatomy and histology of the copulatory apparatus are central for the identification and systematics of these organisms (e.g. E. M. Froehlich, 1955; Negrete & Brusa, 2016). Nonetheless, when traditional, morphology-based taxonomic approaches had been complemented with molecular methodologies in different studies, some nominal species were found to be polyphyletic (Sluys et al., 2016; Carbayo et al., 2018; Almeida, Marques & Carbayo, 2019). Reanalyses of the morphological evidence in those cases revealed that morphological variation assumed to represent within-species polymorphisms, turned out to signal distinct species. From another perspective, reinterpretation of intra-specific morphological variation revealed pseudocryptic species (see references above; Sáez & Lozano, 2005).

The systematics of Geoplaninae above the species level has also benefited from the molecular approach. Molecular phylogenetic analyses of this group revealed a number of polyphyletic genera, one of them, *Geoplana* Stimpson, 1857 was subsequently split into several genera (Carbayo et al., 2013). *Cratera* Carbayo et al., 2013 emerged from *Geoplana* as a monophyletic group with 9 species to which were gradually added another 9 species with similar features. The most conspicuous diagnostic feature of *Cratera* is an ejaculatory duct with its distal

section dilatated (Marcus, 1951; Lago-Barcia & Carbayo, 2018). However, this feature is not found in all members of the genus, probably as a result of a secondary loss (Lago-Barcia & Carbayo, 2018).

In the course of extensive land planarian samplings across the Atlantic forest we have found many individuals that can be attributed to the *Cratera* genus, most of them presenting very similar or even identical features in their external aspect or their internal anatomy. Given the precedents of the existence of cryptic, or pseudocryptic species in other land planarian genera, we set an integrative taxonomic analysis to unveil eventual cryptic species. We adopted the General Lineage Species Concept, that defines species as independently evolving metapopulation lineages (de Queiroz, 1998). To implement this concept, we have used an integrative approach to species delimitations. We applied molecular species delimitation methods to delineate a Primary Species Hypothesis (PSH) based on discovery methods, and thereafter applied a validation method to formulate the Secondary Species Hypothesis (SSH; Puillandre et al. 2012a). We then searched whether the putative species presented morphological features giving support to their validity or not. By doing so we unveiled four species for which molecular and morphological data are coherent with each other. Molecular data of a putative fifth species did not fully support its distinctness, but morphological data did; in this case we gave priority to the latter line of evidence to propose a new species.

## Materials & Methods

### Specimens sampling and morphological study

Intensive samplings were performed in four localities (75 hours sampling in Campos do Jordão; 200 hours sampling in the remaining localities). Field experiments were approved by COTEC - Instituto Florestal do Estado de São Paulo (Proc. SMA 12.640/2011), Museu de



Zoologia (EBBAut.020/2013) and Instituto Chico Mendes de Conservação da Biodiversidade (Proc. 32779-1; 11748-4). Animals were collected from the soil litter during the day and at night. The worms were photographed and, subsequently, killed in boiling water, after which a small tissue sample was taken and preserved ~~it~~ in 100% ethanol for DNA extraction. Vouchers of frozen tissues are kept in FC's laboratory. The remaining part of the body was fixed in 10% formalin and, subsequently, transferred to 80% ethanol. Parts of the body were embedded in paraffin Histosec®, sectioned at 2-7 µm, mounted on glass slides, and subsequently stained with Mallory method as modified by Cason (1950). Slides were examined with a compound microscope. Reconstruction drawings were done with a camera lucida attached to the microscope. Photomicrographs were taken with the help of a digital camera attached to the microscope. Enhancement of the contrast of the microphotographs and a whitish background of the photomicrographs were done with GIMP (GNU Image Manipulation Program 2.8.16; The GIMP team [www.gimp.org](http://www.gimp.org), 1995-2016). Drawings and photomicrographs of sagittal and horizontal views are orientated with anterior to the left. The width of the creeping sole was measured on transverse sections of the pre-pharyngeal region. Type material was deposited in the Museu de Zoologia da Universidade de São Paulo (MZUSP).

The electronic version of this article in Portable Document Format (PDF) will represent a published work according to the International Commission on Zoological Nomenclature (ICZN), and hence the new names contained in the electronic version are effectively published under that Code from the electronic edition alone. This published work and the nomenclatural acts it contains have been registered in ZooBank, the online registration system for the ICZN. The ZooBank LSIDs (Life Science Identifiers) can be resolved and the associated information viewed through any standard web browser by appending the LSID to the prefix <http://zoobank.org/>. The

LSID for this publication is: urn:lsid:zoobank.org:pub:F6B30CB7-6114-434F-9B2A-A2F4CE625A20. The online version of this work is archived and available from the following digital repositories: PeerJ, PubMed Central and CLOCKSS.

# **Molecular data acquisition**

Extractions of genomic DNA were performed using the Wizard® Genomic DNA Purification kit (Promega, Madison, WI, USA) following Álvarez-Presas et al. (2011). Two mitochondrial and four nuclear markers were selected. The mitochondrial markers are a cytochrome oxidase I gene fragment (hereafter referred to as COI), and a mitochondrial fragment which includes the end of the nad4 gene, ~~all the~~ sequence of trnF and the beginning of the cox1 gene. This latter marker, hereafter referred to as Nd4toCox1, is tested for the first time in this work. The four nuclear genes correspond to the 18S rDNA type II (18S), a fragment of the 28S rDNA (28S), a partial coding region of the elongation factor 1-alpha gene (hereafter referred to as EF), and an anonymous nuclear marker (hereafter referred as Tnuc813) developed from NGS data (as ~~exposed~~ in Leria et al., 2019) and tested here for the first time. Primers used to amplify and sequence the genes are ~~available~~ in Table S1. For some individuals (indicated in Table 1), it was not possible to obtain a long COI sequence (~900 bp) of good quality (fragment amplified by the BarS / COIR primers). To overcome this situation, a shorter fragment (COIF / COIR primers), of ~300 bp, was amplified. The polymerase chain reaction (PCR) amplification (25 µL) was performed on a Techne® TC-5000TM (Bibby Scientific Ltd, Staffordshire, UK) and on an Eppendorf Mastercycler® (Eppendorf, Hamburg, Germany) personal thermocyclers using initial denaturation step of 5 min at 92–95 °C, followed by 30–35 cycles of 30- to 50-s denaturation at 94–95 °C, 30- to 45-s annealing at 44–54 °C and 50-s – 1-min extension at 72 °C, with a final

extension step of 3–4 min at 72 °C. The PCR results were verified using electrophoresis of the amplification products on 1% agarose gels stained with GelRed (Biotium, Hayward, CA, USA), and visualized under UV transillumination. Amplification products were purified with a vacuum manifold (Multiscreen®HTS Vacuum Manifold; Millipore Corporation, Billerica, MA, USA). Purification products were sent to Macrogen (Amsterdam, Europe), where both strands were sequenced by Sanger sequencing. Chromatograms were revised and contigs constructed in Geneious v 8.1.7. software (Biomatters; available from <http://www.geneious.com>).


For all the coding genes (COI, Nd4toCox1, EF and Tnuc813), sequences were aligned based on the amino acid sequences using Clustal W (included in the BioEdit software 7.0.9.0 (Hall, 1999)). The genetic code 9 (Echinoderm and flatworms' mitochondrial) was used for translating the mitochondrial genes. Ribosomal RNA gene sequences were aligned using the online version of the software Mafft v7 (Katoh, Rozewicki & Yamada, 2017) applying the G-INS-i iterative refinement method. Misaligned or ambiguously aligned regions were removed using Gblocks v0.91b program (Talavera & Castresana, 2007) allowing 50 as a maximum number of contiguous non-conserved positions and setting the minimum length of a block to 4, and half gap positions allowed. Three different datasets were used for several analyses: (1) *COI* dataset including COI sequences used for the ABGD and mPTP molecular species delimitation approaches; (2) *BPP* datasets 18S, 28S, COI, Nd4toCox1, Tnuc813, and EF independent alignments (completing some sequences with missing data (Ns); see Table 1) used for the BPP molecular species delimitation analysis; and (3) *concatenated* dataset, including the information of the six genes (18S, 28S, EF, Tnuc813, COI and Nd4toCox1) and was used to infer a general phylogeny.

For the individual gene alignments DNA sequence evolution model that better fits the data was estimated by using jModelTest v2.1.4 (Darriba et al., 2012), applying the Akaike information criterion (AIC). For the concatenated dataset PartitionFinder2 version 2.1.1 (Lanfear et al., 2017) was run on the CIPRES Science Gateway (Miller, Pfeiffer & Schwartz, 2010) to identify an appropriate partition scheme and their corresponding DNA evolutionary models. The data were divided by gene, with unlinked branch lengths, the 'raxml' models for selection and the AICc model selection criteria with the 'greedy' search algorithm. The phylogenetic trees for the concatenated dataset were inferred using the Bayesian Inference (BI) method using MrBayes software v3.2.6. (Ronquist et al., 2012) implemented in CIPRES and using BEAGLE (Ayres et al., 2012), setting the evolutionary model and appropriate partitions according to the PartitionFinder results with the unlinked parameters. Two runs of four chains were applied producing 5 million generations and, for each of them, 5,000 trees were stored. It was checked that the probability values (logarithm) of the cold chain reached the stationarity state and the convergence of the two runs, verifying that the average standard deviation of the split frequencies was lower than 0.01. A default burn-in of 25% was used and a consensus tree was obtained from the remaining trees. The maximum likelihood (ML) method was used to infer phylogenies with the software IQtree v1.6.10 (Nguyen et al., 2015). The IQtree searches were carried out using the default configuration in CIPRES, with a starting random tree (option -t RANDOM), and assessing branch support using 1000 ultrafast bootstrap approximation replicates (Minh, Nguyen & Von Haeseler, 2013). The best fit models for each partition were the selected by PartitionFinder and each partition was allowed to have its own set of branch lengths (option -sp).

# **Molecular species delimitation**

For the molecular species delimitation analyses, two discovery methods (ABGD and mPTP) and one validation method (BPP) were applied. Using the COI dataset, the Automatic Barcode Gap Discovery (ABGD) method (Puillandre et al., 2012b) was applied through the website <http://www.wabi.snv.jussieu.fr/public/abgd/abgdweb.html>. The default values of  $P_{min} = 0.001$  and  $P_{max} = 0.10$ , steps = 10 and number of intervals = 20 were used. Using the relative gap width value ( $X$ ) = 1.0 and correcting the distance matrix under the K80 Kimura model with a  $MinSlope = 1.5$ .

The multi-rate Poisson Tree Process (mPTP), which is another single locus analysis, was also used. This model incorporates different levels of intraspecific genetic diversity derived from differences in the evolutionary history or in the sampling of each species, accommodating different coalescence rates within the lineages (Kapli et al., 2017). mPTP analysis was performed in a ML tree reconstructed by IQtree in CIPRES with the *COI* dataset (Suppl Fig. 1). For this analysis the command line version of the mPTP v 0.2.4. software was used without considering the outgroup. Four independent runs of 5,000,000 Monte Carlo Markov chains (MCMC) were carried out sampling every 10,000 generations.

The use of these discovery methods leads to the Primary Species Hypothesis (PSH), used as starting point for the validation step. 

For the validation step, a Bayesian multilocus method of delimiting species (Yang & Rannala, 2010, Yang & Rannala, 2014) implemented in the BPP v3.3 software (Yang, 2015) was applied. Different hypotheses of species delimitation and estimation of the posterior probability (PP) of each model were tested using reversible jump MCMC (rjMCMC). The previous species assignment resulting from the ABGD discovery analysis was used as a starting hypothesis for the

BPP analysis, because it was the analysis that gave the largest number of PSHs. Some species were excluded from this validation analysis ~~since~~ only one individual was available ~~for each one~~ (*Cratera arucuia* Lago-Barcia & Carbayo, 2018 and *Cratera picuia* Lago-Barcia & Carbayo, 2018) or because it only had COI gene sequenced (*Cratera ochra* Rossi et al., 2016) . As they were not the target species for our study, their removal from the analysis was not relevant. A guide tree generated by 100 million generations (stored every 5000) in \* BEAST2 v2.5.2 (Bouckaert et al., 2014) was built in CIPRES with the six single gene datasets (*BPP* datasets), applying the evolutionary model for each gene resulting from the previous jmodeltest analysis (18S=GTR+I; 28S=HKY+I+G; Cox1=GTR+G; EF=GTR+I+G; Nd4toCox1=HKY+I+G and Tnuc=GTR+I).

The molecular clock was set as ~~log-normal-relaxed~~ for all markers (unlinked) and the Birth and Death model was used for **speciation**. In the BPP analysis, both the size of the ancestral population ( $\theta$ ) and the time of origin for each species ( $\tau$ ) were parameterized with four different models (named M1-M4): M1 for large ancestral population size and deep divergence G (1, 10) (for  $\theta$  and  $\tau$ ); M2 for small ancestral population size and shallow divergence G (2, 1000) (for  $\theta$  and  $\tau$ ); M3 for large ancestral population size and shallow divergence (G (1 10) for  $\theta$  and G (2 1000) for  $\tau$ ); and M4 for small ancestral population size and deep divergence (G (2 1000) for  $\theta$  and G (1 10) for  $\tau$ ). Under the algorithm 0 it was run the rjMCMC analysis in 100,000 generations (with a sampling interval of 2) excluding 10% as burn-in. To test the robustness of the results, these executions were replicated using different starting seeds. These analyses were done without outgroup. Results of BPP lead to ~~the~~ Secondary Species Hypothesis (SSH).

## Abbreviations used in figures

219 (cg) cyanophil gland cells  
 220 (co) common glandular ovovitelline duct  
 221 (e) eye  
 222 (ed) dilatated portion of ejaculatory duct  
 223 (ej) ejaculatory duct  
 224 (ep) esophagus  
 225 (fa) female atrium  
 226 (fc) female genital canal  
 227 (fo) fold  
 228 (g) gonopore  
 229 (gl) glands  
 230 (i) intestine  
 231 (lc) longitudinal cutaneous muscle fibers  
 232 (m) muscle fiber  
 233 (ma) male genital atrium  
 234 (mc) common muscle coat  
 235 (mo) mouth  
 236 (o) ovary  
 237 (ov) ovovitelline duct  
 238 (ph) pharyngeal pouch  
 239 (pb) penis bulb  
 240 (pp) penis papilla  
 241 (px) pharynx



242 (sb) subintestinal transverse muscle fibers  
 243 (sd) sperm duct  
 244 (sg) shell glands  
 245 (sp) suprainestinal transverse muscle fibers  
 246 (t) testis  
 247 (vi) vitellaria  
 248 (vn) ventral nerve plate

249

## 250 **Results**

### 251 **Molecular datasets**

252 The *COI* dataset consists of 40 sequences with a length of 822 bp, ~~and~~ the concatenated  
 253 dataset (28 *Cratera* sequences plus 3 outgroups from the genus *Obama*) has a length of 5671 bp.  
 254 The individual gene datasets for the \*BEAST analysis are constituted by 26 sequences with a  
 255 length of 1349 bp (18S), 1544 bp (28S), 825 bp (COI), 612 bp (EF), 730 bp (Nd4toCox1) and  
 256 611 bp (Tnuc813).

257

### 258 **Phylogenetic analysis**

259 The partitions obtained with PartitionFinder and applied to the phylogenetic analysis of  
 260 the *concatenated* dataset are Cox1\_codon2, EF\_codon2, 18S, Tnuc813-1\_codon3, Tnuc813-  
 261 3\_codon2, Tnuc813-3\_codon3, Tnuc813-5\_codon1, Tnuc813-5\_codon2, Tnuc813-5\_codon3 =  
 262 K81UF + G, 28S = TIM + G, Cox1\_codon1, EF\_codon1 = TRN + G, Cox1\_codon3 = GTR + G,  
 263 EF\_codon3, Tnuc813-1\_codon2, Tnuc813-3\_codon1 = TVM + G, Nd4toCox1-1\_codon1,  
 264 Nd4toCox1-1\_codon2, Nd4toCox1-3\_codon1, Nd4toCox1-3\_codon3, Tnuc813- 1\_codon1 =  
 265 GTR + G, Tnuc813-2, Tnuc813-4 = GTR + G, Nd4toCox1-1\_codon3, Nd4toCox1-2,



Nd4toCox1-3\_codon2 = HKY + G. For the concatenated analyses, the topology obtained is the same in both methods (ML and BI) as shown in Fig. 2. There is only a small difference in the relationships between the specimens within two of the new species described in the present paper (*Cratera piguaiatui* sp. nov. and *C. piguaiassu* sp. nov.), but without statistical support for any of the two methods. All known species are monophyletic. The new species described here (*C. piguaiatui* sp. nov., *C. imbiri* sp. nov. and *C. paraitinga* sp. nov.) are sister species, forming a large monophyletic group, which in turn is sister to the species *C. cuarassu* Carbayo & Almeida, 2015. *Cratera pseudovaginuloides* (Riester, 1938) is a sister lineage of the new species described here, *C. piguaiaboja* sp. nov., both constituting the sister group of a large clade formed by the species *C. piguaiassu* sp. nov. and *C. crioula* (Froehlich, 1955) on the one hand and the group constituted by the three species *C. picuia*, *C. arucuia* and *C. tamoia* (Froehlich, 1955). The vast majority of the relationships present high support values at the nodes for both methodologies (PP and bootstrap values).

## Molecular species delimitation

On the concatenated tree in Fig. 2 is displayed a summary of the species delimitation results. The ABGD method delimits within the *Cratera* genus 13 Molecular Operational Taxonomic Units (MOTUs) with a p-value of P 0.001 - 0.0046. The mPTP method delimits 11 candidate species for the ingroup with average support of 0.90. In both delimitations, mPTP and ABGD, *C. ochra* is delimited as a single candidate species. However, it is not present in the concatenated tree in Fig. 2 because there are only COI sequences in GenBank for this species (Table 1 and Suppl Fig. 1). For this same reason the species is not included in the BPP analyses. ABGD predicts a higher number of candidate species than mPTP. In consequence,

ABGD ~~candidate~~ set of species is adopted as a reference to designate the PSHs in order to test as many scenarios as possible in the validation with the BPP method. The assignment is as follows. All known species are delimited by both ABGD and mPTP methods as candidate species. Hence, each is assigned a PSHs (PSH-4 is *C. cuarassu*, PSH-5 is *C. crioula*, PSH-8 is *C. tamoia* and PSH-10 corresponds to *C. pseudovaginuloides*). Regarding the rest of *Cratera* individuals included in this work, the two discovery methods coincide in assigning individuals F2789, F2809, F5178 F2040, F2031, F2054 to one candidate species (PSH-1) and individuals F2828 and F2829 to another candidate species (PSH-9). Finally, in two cases a clade that mPTP considers as a single MOTU is divided in two candidate species by ABGD ~~these are~~ designated as candidate species PSH-2, PSH-3, PSH-6 and PSH-7. The species *C. picuia* and *C. arucuia* are not assigned any PSH because they are singletons (constituted by a single individual) and ~~so~~ are not included in the validation step. ~~So, finally~~ 10 PSHs ~~are set~~ to be validated in BPP.

The species tree resulting from the \*BEAST analysis (Fig. 3), used as the input tree to implement the BPP method, differs slightly from the tree inferred using the concatenated dataset. In the ML and BI phylogenies inferred from the concatenated dataset (Fig. 2), the clade formed by PSH-9 and PSH-10 is sister to the clade constituted by PSH-5, PSH-6, PSH-7 and PSH-8. However, in the \*BEAST tree PSH-9 + PSH-10 ~~is sister group~~ of the rest of species. The small differences could be due to the fact that *C. picuia* and *C. arucuia* were not included in the \*BEAST analysis, but ~~this~~ does not affect the subsequent species assignment.

The different values of  $\theta$  (ancestral population size) and  $\tau$  (time of divergence) that are used in the 4 BPP analyses (M1, M2, M3 and M4) do not have a significant effect on the results of the BPP analyses (Fig. 3), except for the node that separates PSH-2 and PSH-3, the PP value of which is higher than 0.95 in the M2 and M4 models (small ancestral population size) and a

little lower than 0.95 in the M1 and M3 models (large ancestral population size). Of the 10 PSHs that are analysed as starting hypothesis for BPP, only 9 are validated since PSH-6 and PSH-7 would form a single SSH (SSH-6 in Fig. 3). In conclusion, the BPP results determine the presence of 9 SSHs, validating five new species of *Cratera* (SSH-1, SSH-2; SSH-3, SSH-6, and SSH-9) that will be described in the following section.

## **Taxonomic account**

### **Order Tricladida Lang, 1884**

### **Suborder Continenticola Carranza et al., 1998**

### **Family Geoplanidae Stimpson, 1857**

### **Genus *Cratera* Carbayo et al., 2013**

### ***Cratera piguaiassu* ~~sp. nov.~~, Araujo, Carbayo, Riutort & Álvarez-Presas**

urn:lsid:zoobank.org:act:DE3D812D-C387-40BD-9273-7BC1FE59D09C

## **Synonymy.**

*Cratera* sp. 1: Carbayo et al. (2013).

**Etymology.** The name *piguaiassu* is a free composition of the Tupi (indigenous Brazilian language) words pyguaia (meaning hole, cave) and assu (meaning large) (Tibiriçá, 1984). It refers to the large distal dilatation of the ejaculatory duct.

**Type locality.** Parque Nacional da Serra da Bocaina, São José do Barreiro, State of São Paulo, Brazil.

**Material studied.** All specimens collected in the Parque Nacional da Serra da Bocaina, São José

do Barreiro, State of São Paulo, Brazil (-22.75, -44.62) by Carbayo et al. Holotype F2825 (MZUSP PL 2150): 8 September 2008. Horizontal sections of pre-pharyngeal region-1 on 5 slides; transverse sections of pre-pharyngeal region-2 on 5 slides; sagittal sections of pharynx and copulatory apparatus on 34 slides. Paratypes: F2025 (MZUSP PL 2146): 5 February 2008. Horizontal sections of pre-pharyngeal region-1 on 15 slides; transverse sections of pre-pharyngeal region-2 on 7 slides. Sagittal sections of copulatory apparatus on 15 slides. F2807 (MZUSP PL 1050): 7 September 2008. Transverse sections of cephalic extremity on 7 slides; horizontal sections of ovaries on 5 slides; transverse sections of pre-pharyngeal region on 6 slides; sagittal sections of pharynx on 12 slides; sagittal sections of copulatory apparatus on 11 slides. F2821 (MZUSP PL 1052): 8 September 2008. Sagittal sections of a piece of the body behind cephalic extremity on 71 slides; sagittal sections of pharynx and copulatory apparatus on 71 slides. F2834 (MZUSP PL 2151): 8 September 2008. Preserved in 80% ethanol.

# **Diagnosis**

Species of *Cratera* 50-62 mm long (34-38 mm preserved); dorsum chestnut brown to black brown, excepting the yellow orange or grayish body margins. A thin grayish median stripe may be present. Eyes dorsal. Pharynx bell-shaped. Penis papilla horizontal; distal portion of ejaculatory duct very dilated to occupy most of the length of the penis papilla. Common glandular ovovitelline duct absent.

# **Description**

When crawling, the longest specimen (paratype F2807), up to 62 mm in length and 3.5 mm in width; preserved, 38 and 7 mm, respectively. Body elongate, slightly lanceolated, with maximum width at the level of the pharynx. Anterior to it, body narrows gradually towards the rounded tip; posterior to the level of the pharynx, body becomes narrower abruptly near

posterior, pointed tip. Dorsum slightly convex, ventral side flattened. Creeping sole as wide as 92-94% of body width at the pre-pharyngeal region. Mouth at a distance from anterior extremity equal to 70% of body length; gonopore at 85 % in holotype. In paratype F2807, 74% and 85%, respectively.

Color of the dorsum varies from chestnut brown (Fig. 4A) to black brown (Fig. 4B). A submarginal yellow orange or grayish stripe is present in anterior tenth of the body; posteriorly, this stripe becomes marginal. The stripe, measuring 8% of body width, may be inconspicuous. A thin grayish median stripe, 4% of body width, may also occur. Ventral surface varies from deep orange (Fig. 4A, inset) to grayish (Fig. 4B, inset).

Each eye is formed by a single pigmented cup 30 µm in diameter. Clear halos around eyes were not observed. Eyes contour anterior extremity of the body in a single row along the first 5 millimeters (equal to 13% of body length, paratype F2807); then they spread onto the back in a lateral band 1/3th of the body width, reaching the posterior tip.

Sensory pits, 15 µm deep, in a uniserial ventro-lateral row, from very anterior tip up to 29% of body length posterior. Dorsal and ventral epidermis in pre-pharyngeal region pierced by necks of two types of cell glands producing erythrophil and cyanophil granules, respectively. Besides, rhabditogen cells discharge their content through dorsal epithelium. Glandular margin constituted by two types of cell glands, one abundant type producing xanthophil granules and a less abundant type secreting erythrophil granules.

Cutaneous musculature constituted of a subepithelial circular layer, followed by two diagonal layers with decussate fibers, and then a strongly developed longitudinal layer with fibers arranged in bundles (Fig. 4C). Longitudinal layer is 40 µm thick dorsally and 50 µm ventrally (paratype F2807); dorsally, fibers gathered into well-delimited and more compact

bundles than ventrally. Thickness of cutaneous muscle ranges from 8.9% (F2807) to 13.4% (F2025).

Three parenchymal muscle layers throughout the body: a dorsal layer of diagonal decussate fibers (20  $\mu$ m thick), a transverse suprainestinal layer (150  $\mu$ m), and a transverse subintestinal one (90  $\mu$ m). Central nervous system as a ventral nerve plate. Cerebral ganglia were not discerned.

Mouth located shortly behind middle of pharyngeal pouch. Pharynx bell-shaped, with dorsal insertion posterior to the ventral at the equivalent of 40% of pharyngeal length (Fig. 4D). Esophagus length, 33% of pharyngeal length. Outer pharyngeal epithelium underlain by a one-fiber-thick layer of longitudinal muscle, followed by a circular one (7  $\mu$ m thick); inner epithelium underlain by a layer (70-150  $\mu$ m) of circular fibers with interspersed longitudinal fibers, followed by a longitudinal muscle layer (10  $\mu$ m). Pharyngeal pouch at 1.6-2.6 mm from prostatic vesicle.

Testes dorsal, located under the suprainestinal transverse muscle layer, partially placed between the intestinal diverticula (Fig. 4C). Sperm ducts run immediately above the subintestinal muscle layer, dorso-medially to the ovovitelline ducts (Fig. 4C). Shortly behind the prostatic

vesicle, sperm ducts curve medially and anteriorly, to communicate separately with the respective short lateral diverticulum of the vesicle (Fig. 5A). Vesicle extrabulbar, tubular, with anterior portion slightly dilated. In lateral view vesicle with the shape of an inverted U, the distal portion of which, anterior to anterior region of penis bulb, communicates with ejaculatory duct.

Prostatic vesicle lined with a ciliated, tall and tortuous epithelium, which is traversed by cells producing fine erythrophil granules. This epithelium surrounded by a circular muscle layer.

Ejaculatory duct straight, running slightly dorsally. At the basis of the penis papilla, duct widens

to give rise to a very large cavity ~~inside the penis papilla~~ (Figs. 5A-C). At the tip of penis papilla this cavity narrows to open into male atrium. Ejaculatory duct lined with a cuboidal, ciliated epithelium and surrounded by a 25- $\mu$ m thick circular muscle layer. Under this muscle layer there is an additional, one-fiber-thick layer of longitudinal muscle.

Penis papilla a long, roughly conical, protrusible organ extending along the length of the male atrium or even beyond (Fig. 5A-C). Lining epithelium of the penial cavity cuboidal, not ciliated, pierced by necks of cell producing minute erythrophil granules ( $<0.2 \mu$ m), and underlain by a layer (25  $\mu$ m) of circular muscle, followed by a simple layer of longitudinal muscle. The penis papilla is clothed with a cuboidal, non-ciliated epithelium, which is traversed by necks of cells producing erythrophil granules and is underlain by a 20- $\mu$ m-thick layer of circular muscle with some interspersed longitudinal fibers.

Male atrium ample and smooth, not narrowed distally. It is lined with a cuboidal, non-ciliated epithelium, which is pierced by necks of cells producing granules with weak xanthophil affinity. Male atrial epithelium underlain by a muscle layer (40  $\mu$ m) of circular fibers.

Ovaries roughly ovoid, with maximum length 400  $\mu$ m anteroposteriorly. They are located immediately above the ventral nerve plate, at a distance from anterior tip equivalent to 21% of body length. Ovovitelline ducts arise from external side of the ovaries, subsequently run backwards above ventral nerve plate. The ducts ascend laterally to the female atrium, posteriorly and medially inclined, to unite dorsally to the atrium (Fig. 5A). Half of the ascending portion of these ducts receives secretion of shell glands. Ovovitelline ducts open the female genital canal. This canal is a long canalicular projection of the posterior portion of the female atrium. ~~This canal is directed forwards~~ (Fig. 5D). Female atrium, as long as male atrium, and funnel-shaped. Lateral walls of female atrium partially occlude its lumen. Its lining epithelium is columnar, and

the free surface of which is erythrophil and displays small recesses that appear as small gaps. In the anterior portion of female atrium, the epithelium is 40  $\mu\text{m}$  high; posteriorly it becomes taller and its nuclei arranged at different heights within the cells, so giving to the epithelium a multilayered aspect. Necks of cells producing erythrophil granules pierce this epithelium, which is clothed with two layers of muscles; clothing the anterior half of the atrium there is a 5- $\mu\text{m}$ -thick circular muscle layer followed by a 3- $\mu\text{m}$ -thick longitudinal one. Arrangement of these layers is inverted in posterior half of female atrium, i. e., a layer (5  $\mu\text{m}$ ) of longitudinal is followed by a layer (20  $\mu\text{m}$ ) of circular fibers.

# Remarks

Regarding the external aspect, *C. tamoia* is the only species of the genus resembling *C. piguaiassu* in that both display a uniform dark dorsum with clear margins. However, although color patterns are alike, *C. piguaiassu* differs in being darker. Moreover, the phylogenetic analyses show that these two species are highly differentiated at the genetic level and do not even represent sister groups. Regarding the internal organs, *C. piguaiassu* is unique among the representatives of *Cratera* in the very large dilatation of the ejaculatory duct. This dilatation occupies most of the penis papilla. This situation is also present in *C. cuarassu*, but the penis papilla of the latter is vertically oriented (vs. horizontally in *C. piguaiassu*). The molecular delimitation methods all clearly point to *C. piguaiassu* being a species differentiated from the rest of species molecularly analysed in the present study. On the other hand, although the primary hypothesis found this lineage could be divided in two species, neither the molecular validation nor the morphological analysis found evidence of this possibility.

*Cratera piguaiaboja* sp. nov., Araujo, Carbayo, Riutort & Álvarez-Presas



urn:lsid:zoobank.org:act:46D76DD7-B129-461D-8803-3E918AA4601C

451

**Etymology.** The name *piguaiaioja* is a free composition of the Tupi (indigenous Brazilian language) words pyguaia (meaning hole, cave) and bojá (meaning intermediate, middle) (Tibiriçá, 1984). It refers to the ~~middle~~ size of the distal dilatation of the ejaculatory duct.

**Type locality.** Parque Nacional da Serra da Bocaina, São José do Barreiro, State of São Paulo, Brazil.


**Material studied.** All specimens collected in Parque Nacional da Serra da Bocaina, São José do Barreiro, State of São Paulo, Brazil (-22.75, -44.62), in September 2008 by Carbayo ~~et al.~~ Holotype F2829 (MZUSP PL 0459): transverse sections of cephalic extremity on 4 slides; horizontal sections of a portion of the body behind cephalic extremity on 4 slides; transverse sections of pre-pharyngeal portion on 7 slides; sagittal sections of pharynx on 6 slides; sagittal sections of copulatory apparatus on 4 slides (~~plus~~ one slide lost). F2828 (MZUSP PL 0458): horizontal sections of a portion behind anterior extremity on 6 slides; transverse sections of the pre-pharyngeal portion on 22 slides; sagittal sections of pharynx on 13 slides; sagittal sections of copulatory apparatus on 14 slides.


# **Diagnosis**


Species of *Cratera* 34 mm long preserved; dorsum olive grey with large black dots, with these being more concentrated in paramedian bands; eyes marginal; pharynx bell-shaped; distal portion of ejaculatory duct dilated to occupy half of the penis papilla; male atrium separated from female by a narrowing; penis papilla shorter than male atrium; prostatic vesicle with inverted-U shape in lateral view; penis papilla postero-dorsally oriented; numerous cyanophil cell necks piercing roof of male atrium; female atrium half the length of the male atrium;


473 common glandular ovovitelline duct absent.

# 474 Description

475  Fixed, holotype measures 34 mm in length and 4 in width. Body elongate, with parallel  
476 margins along most of body length. Anterior extremity rounded; posterior pointed. Dorsal side  
477 convex; ventral side flattened. Creeping sole, 95% of body width at the pre-pharyngeal region.  
478 Mouth at a distance from anterior extremity equal to 71% of body length; gonopore at 87%  
479 (holotype).

480 Dorsum spotted black on olive grey ground color (Fig. 6A-D). Large black  spots join  
481 each other. Spots distributed all over dorsum and especially concentrated in a median band (33%  
482 of body width). This band may be divided by a thin midline, measuring 6% of body width (Fig.  
483 6C). Ventral surface olive gray (Fig. 6A), gray at anterior extremity.

484 Each eye is formed by a single pigmented cup 40   $\mu$ m diameter. Clear halos around  
485 eyes ~~were not found~~. Eyes contour anterior extremity in a single row, posteriorly they are  
486 arranged marginally ~~until~~ posterior tip of the body.

487 Sensory pits were not found despite intensive search on the sections,  which are partially  
488 damaged. Dorsal and ventral epidermis in pre-pharyngeal region pierced by necks of two types  
489 of ~~cell glands~~ producing ~~granules~~, erythrophil and cyanophil, respectively. ~~Besides~~, rhabditogen  
490 cells discharge their content through dorsal epithelium and, ~~scarcely~~, ventral epithelium as well.  
491 Glandular margin not well defined (Fig. 7A), constituted by three types of ~~cell glands~~, one  
492 abundant type producing xanthophil granules and a less abundant type secreting erythrophil  
493 granules, and rhabditogen cells.

494 Cutaneous musculature constituted of a subepithelial circular layer, followed by two  
495 diagonals with decussate fibers, and then a strongly developed longitudinal layer with fibers

496 arranged in bundles (Fig. 7A). Longitudinal layer 55  $\mu\text{m}$  thick dorsally and 90  $\mu\text{m}$  ventrally.

497 Fibers of this layer are gathered into well-delimited and more compact bundles than ventrally.

498 Thickness of cutaneous muscle, 12.5% of body height (holotype).

499 Three parenchymal muscle layers throughout the body: a dorsal layer of diagonal  
500 decussate fibers (20  $\mu\text{m}$  thick, holotype), a transverse suprainestinal layer (60  $\mu\text{m}$ ), and a  
501 transverse subintestinal one (70  $\mu\text{m}$ ). Central nervous system as a ventral nerve plate. Cerebral  
502 ganglia starting at 0.5 mm from anterior extremity (1.5% of body length, holotype).

503 Mouth located at the end of second third of pharyngeal pouch (Fig. 7B). Pharynx bell-  
504 shaped, with dorsal insertion posterior to the ventral at the equivalent of 36% of pharyngeal  
505 length. Esophagus length, 21% of pharyngeal length. Outer pharyngeal epithelium underlain by a  
506 one-fiber-thick longitudinal muscle layer followed by a circular one (4  $\mu\text{m}$  thick); inner  
507 epithelium underlain by a circular muscle layer (30-60  $\mu\text{m}$  thick), followed by a longitudinal  
508 muscle one (5  $\mu\text{m}$ ). Pharyngeal pouch of holotype at 2.5 mm (equivalent to 7% of body length)  
509 from prostatic vesicle.

510 Testes dorsal, located under the suprainestinal transverse muscle layer, partially placed  
511 between the intestinal diverticula (Fig. 7A). Posteriormost testes lateral to insertion of the  
512 pharynx. Sperm ducts run immediately above the subintestinal muscle layer, dorso-medially to  
513 the ovovitelline ducts (Fig. 7A). Below prostatic vesicle, sperm ducts curve medially and  
514 anteriorly, to communicate separately with the respective short lateral diverticulum of the  
515 vesicle. Prostatic vesicle extrabulbar and tubular. In lateral view, this vesicle is seen as an  
516 inverted U. Prostatic vesicle approaches anterior region of penis bulb and communicates with  
517 ejaculatory duct. Ventral portion of penis bulb posterior to dorsal portion.

518 Prostatic vesicle lined with a ciliated, columnar epithelium, traversed by necks of two

types of cell producing erythrophil and cyanophil granules, respectively; the cyanophil glands being much more abundant (Fig. 8A). Epithelium of prostatic vesicle surrounded by a 130- $\mu$ m-thick circular muscle layer. Proximal portion of ejaculatory duct sinuous; distal portion straight, traversing center of penis papilla; midway of penis papilla, ejaculatory duct widens to give rise to a relatively large, funnel-shaped cavity, which opens at the tip of the penis papilla (Fig. 7C-D, 8A). Ejaculatory duct lined with a cuboidal, ciliated epithelium; in its dilated portion, pierced by necks of cells producing xanthophil granules. Epithelium of ejaculatory duct surrounded by a 20- $\mu$ m thick circular muscle layer.

Penis papilla conical cylindrical, 1.3-1.5 times longer than its diameter and as long as the male atrium or shorter (Fig. 7C-D). Penis papilla clothed with non-ciliated epithelium. Columnar epithelium lines basal half of papilla; cuboidal epithelium lines distal half. Epithelium of papilla pierced by necks of three types of cells producing erythrophil, xanthophil and cyanophil granules, respectively (but the latter appears erythrophil in paratype); necks of cyanophil glands only piercing epithelium of basal half of penis papilla. Epithelium of penis papilla underlain by a 10- $\mu$ m-thick layer of circular muscle fibers followed by a longitudinal layer, 10  $\mu$ m thick.

Parenchyma of penis papilla richly traversed by circular and longitudinal muscle fibers.

Male atrium ample and smooth, lined with a columnar, non-ciliated epithelium. Epithelium clothing roof of male atrium pierced by very numerous necks of cells producing cyanophil granules. Ventral portion of male atrium pierced by necks of glands producing erythrophil granules. Atrial epithelium underlain by a layer (12  $\mu$ m thick) of circular muscle fibers, followed under dorsal epithelium by a 5- $\mu$ m-thick longitudinal muscle layer.

Ovaries were not found in histological sections and were probably destroyed in the portion from which a tissue sample was extracted. Ovovitelline ducts ascend laterally to

proximal portion of the female atrium, posteriorly and medially inclined. Subsequently, the ducts unite dorsally to the posterior portion of atrium. Half of ascending portion of these ducts receives shell glands. Ovovitelline ducts open into female genital canal, i.e., a common glandular ovovitelline duct is absent. Female genital canal projects forwards from the postero-dorsal portion of the female atrium. Female atrium ample, 55-57% the length of male atrium and lined with 30-70  $\mu\text{m}$  high, non-ciliated epithelium, with stratified aspect. Surface of epithelium sinuous; subapical portion of epithelial cells cyanophil (Fig. 8B) or erythrophil (Fig. 8C). Necks of two types of cells, producing erythrophil and cyanophil granules, respectively, pierce this epithelium, which is underlain by a 25- $\mu\text{m}$  thick and dense layer of circular muscle, followed by a 3  $\mu\text{m}$  thick longitudinal muscle layer.

# Remarks

*C. piguaiaboja* is distinctive among all species of the genus in the spotted color pattern of the dorsal side. Regarding its copulatory apparatus, there are five species with a similar aspect of the copulatory apparatus and size of the dilatation of the ejaculatory duct, namely, *C. aureomaculata* Rossi & Leal-Zanchet, 2017, *C. nigrimarginata* Rossi & Leal-Zanchet, 2017, *C. pseudovaginuloides*, *C. tamoia*, and *C. viridimaculata* Negrete & Brusa, 2016. However, (a) all of these five species have a common glandular ovovitelline duct (~~vs.~~ absent in *C. piguaiaboja*; but see redescription of *C. pseudovaginuloides* in Riester, 1938); (b) the male and female atria are not separated by a constriction in *C. pseudovaginuloides* (~~vs.~~ separated in *C. piguaiaboja*); (c) the penis papilla is longer than the male atrium in *C. nigrimarginata* and *C. pseudovaginuloides* (~~vs.~~ shorter in *C. piguaiaboja*); (d) the prostatic vesicle is horizontal in *C. nigrimarginata* (~~vs.~~ inverted-U shaped in *C. piguaiassu*); (e) the female atrium is funnel-shaped, and its posterior section oriented upwards in *C. viridimaculata* (~~vs.~~ horizontal, and not funnel-

shaped in *C. piguaiaboja*); (f) the prostatic vesicle runs postero-dorsally in *C. aureomaculata* and *C. tamoi* (~~vs.~~ inverted U-shaped in *C. piguaiaboja*); (g) the penis papilla exhibits a postero-ventral orientation in *C. tamoi* (~~vs.~~ postero-dorsal in *C. piguaiaboja*); and (h) there is no accumulation of necks of cyanophil cells piercing the roof of the male atrium in *C. nigrimarginata*, *C. pseudovaginuloides*, and *C. tamoi* (~~vs. present~~ in *C. piguaiaboja*).

The phylogenetic tree as well as the molecular species delimitation analyses also show that this species is distinct and well-delimited from *C. pseudovaginuloides* and *C. tamoi*, the two species included in these analyses that show similarities with *C. piguaiaboja*.

***Cratera piguaiatui* sp. nov., Araujo, Carbayo, Riutort & Álvarez-Presas**

urn:lsid:zoobank.org:act:FB96BE96-86AD-41FB-961F-C0337C56A596

**Synonymy.** *Cratera* sp. 4: Carbayo et al. (2013).

**Etymology.** The name *piguaiatui* is a free composition of the Tupi (indigenous Brazilian language) words pyguaia (meaning hole, cave) and tui (meaning tiny, insignificant) (Tibiriçá, 1984). It refers to the small distal dilatation of the ejaculatory duct.

**Type locality.** Parque Nacional da Serra da Bocaina, São José do Barreiro, State of São Paulo, Brazil.

**Distribution.** Parque Nacional da Serra da Bocaina, São José do Barreiro, State of São Paulo; Parque Nacional Itatiaia, Resende, State of Rio de Janeiro, Brazil.

**Material studied.** Holotype F2809 (MZUSP PL 1051): Parque Nacional da Serra da Bocaina, São José do Barreiro, State of São Paulo (-22.75, -44.62). F. Carbayo et al., 7 September 2008; transverse sections of cephalic extremity on 4 slides; sagittal sections of a portion immediately

588 behind cephalic extremity on 19 slides; horizontal sections of a immediately behind on 12 slides;  
 589 transverse sections of pre-pharyngeal on 16 slides; sagittal sections of pharynx on 17 slides;  
 590 sagittal sections of copulatory apparatus on 23 slides. Paratypes: F2031 (MZUSP PL 1014):  
 591 Ibidem, 7 September 2008; sagittal sections of copulatory apparatus on 6 slides. F2054 (MZUSP  
 592 PL 2148): Ibidem, 9 September 2008; sagittal sections of pharynx and copulatory apparatus on  
 593 13 slides (~~including 3 slides lost~~). F2040 (MZUSP PL 2147): Ibidem, 9 February 2007,  
 594 preserved in 80% ethanol. F2798 (MZUSP PL 2149): Ibidem, 7 September 2008; preserved in  
 595 80% ethanol. F5178 (MZUSP PL 2154): Parque Nacional de Itatiaia, Resende, State of Rio de  
 596 Janeiro (-22.43328, -44.61539), Brazil, F. Carbayo et al., 5 April 2012, horizontal sections of a  
 597 body portion behind cephalic extremity on 7 slides; transverse sections of pre-pharyngeal on 15  
 598 slides; sagittal sections of pharynx on 17 slides; sagittal sections of copulatory apparatus on 30  
 599 slides.

## 600 **Diagnosis**

601 Species of *Cratera* 45-70 mm long ~~preserved~~; dorsum with a melon yellow median stripe,  
 602 bordered on either side by a jet-black stripe external to which a marginal traffic white stripe;  
 603 body margins jet black. Anterior 1/5th of the body colored with a gradient of carmine red; eyes  
 604 marginal; pharynx cylindrical; distal dilatation of ejaculatory duct relatively small; pharyngeal  
 605 pouch 0.6 mm anterior to the prostatic vesicle (equal to 1% of body length); penis papilla shorter  
 606 than male atrium; female atrium 2.5 times longer than the male atrium; common glandular  
 607 ovovitelline duct long.

## 608 **Description**

609 Preserved 45-58 mm in length and 7 mm in width. Body slightly lanceolate, with  
 610 maximum width at the level of the pharynx. Anterior to it, body ~~becomes thinner~~ gradually to the

rounded tip; posterior to the level of the pharynx, body ~~becomes thinner~~ abruptly close to posterior ~~pointed~~ tip. Dorsum slightly convex, ventral side flattened. Creeping sole, 95% of body width at pre-pharyngeal region. Mouth at a distance from anterior extremity equal to 73% of body length; the gonopore at 82% (holotype).

Dorsum with a melon yellow median stripe, 28% of body width, which is bordered on either side by a jet-black stripe, 22% of the body width (Fig. 9A-B). External to jet black stripes, a traffic white marginal stripe, 10% of body width; body margin (3% of the body width) jet black. Anterior 1/5th of the body colored with a gradient of carmine red, dorsally and ventrally; otherwise, ventral side grey white (Fig. 9B).

Each eye is formed by a single pigmented cup with 35  $\mu$ m in diameter. No clear halos around eyes. Eyes contour the anterior extremity in a single row and ~~extend marginally~~ until posterior tip.

Sensory pits, 20  $\mu$ m deep, as a uniserial ventro-lateral row, from anterior extremity ~~through a body length~~ at least equal to 9% of body length (holotype). ~~Besides~~ rhabditogen cells, necks of two types of ~~cell glands~~, producing xanthophil and erythrophil granules, respectively, pierce prepharyngeal dorsal epithelium; the latter also pierce ventral epithelium. Conspicuous glandular margin constituted of abundant glands producing erythrophil granules (Fig. 10A).

Cutaneous musculature of three layers: a subepithelial circular layer, followed by two diagonals with decussate fibers, and then a strongly developed longitudinal, 30  $\mu$ m thick dorsally and 40  $\mu$ m thick ventrally (holotype). Fibers of the longitudinal layer gathered in bundles which are dorsally better delimited than ventrally. Relative thickness of cutaneous muscle, 9.1% (holotype).

Three parenchymal muscle layers throughout the body, all constituted by fibers relatively



densely packed: a dorsal layer of diagonal decussate fibers (15  $\mu\text{m}$  thick, holotype), a transverse suprainestinal layer (25  $\mu\text{m}$ ), and a transverse subintestinal one (25  $\mu\text{m}$ ).

Central nervous system as a ventral nerve plate. Clearly evident cerebral ganglia were not found.

Mouth in middle of pharyngeal pouch (Fig. 10B). Pharynx cylindrical, with dorsal insertion posterior to the ventral at the equivalent of 20% of pharyngeal length (paratype F2054). Esophagus length, ca. 10% of pharyngeal length (paratype F2054). Outer pharyngeal epithelium underlain by a one-fiber-thick layer (4  $\mu\text{m}$ ) of longitudinal muscle fibers followed by a layer of circular fibers (7  $\mu\text{m}$ ); inner pharyngeal epithelium underlain by a layer (80  $\mu\text{m}$ ) of circular fibers, followed by a layer (10  $\mu\text{m}$ ) of longitudinal fibers (holotype). Pharyngeal pouch at 600  $\mu\text{m}$  from prostatic vesicle in holotype (or 1% of body length).

Testes dorsal, located under suprainestinal transverse muscle layer, partially placed between the intestinal diverticula. The testes extend from level of ovaries to nearly root of pharynx. Distal course of sperm ducts running posteriorly and medially to communicate with the respective lateral diverticulum of the prostatic vesicle (Fig. 11A). Paired portion represents ca. half of the total length of this organ. This vesicle, extrabulbar, approximately pear-shaped in lateral view, with posterior portion running posteriorly and upwards until anterior region of penis bulb. Vesicle lined with a ciliated epithelium, which is pierced by necks of cells producing fine erythrophil granules. A 20  $\mu\text{m}$  thick layer of circular muscle fibers surrounds vesicle. Inside penis papilla vesicle communicates with a horizontal, initially sinuous ejaculatory duct which is lined with a cuboidal, ciliated epithelium. This epithelium surrounded by a 5  $\mu\text{m}$  thick layer of circular muscle fibers. Near tip of penis papilla, lumen of the ejaculatory duct doubles its width to form a small cavity (Fig. 11A-C).

Penis papilla short, horizontally placed, and roughly bulb-shaped; shorter than male atrium (Fig. 11A-B). Male atrium slightly folded. Penis papilla and male atrium clothed with a cuboidal non-ciliated epithelium, this pierced by necks of two types of cells, producing erythrophil and xanthophil granules, respectively. Epithelium of penis papilla and that of male atrium underlain by a 7- $\mu$ m-thick layer of circular muscle fibers, followed by a 7- $\mu$ m-thick layer of longitudinal muscle fibers.

Ovaries elongate, roughly ovoid, with 250  $\mu$ m anteroposteriorly. They are located immediately above the ventral nerve plate, at a distance from anterior tip equivalent to 30% of body length (holotype). Ovovitelline ducts arise from dorso-external side of ovaries and run backwards above the ventral nerve plate. They ascend laterally to female atrium to unite common glandular ovovitelline duct dorsally to female atrium. Distal ascending portion of these ducts receive shell glands. Common glandular ovovitelline duct long (1.2 mm, ie., 1/3th of the length of female atrium in holotype) communicating with female genital canal, the latter being a projection of the posterior portion of female atrium directed forwards and dorsally. Female atrium funnel-shaped, with a length 2.5 times that of male atrium. Lateral wall of female atrium with folds narrowing its lumen. Female atrium lined with a non-ciliated, 25  $\mu$ m tall epithelium along anterior 4/5th of its length. Posterior 1/5th lined with a 50- $\mu$ m-high epithelium that might display a multilayered one; quality of the sections precluded confirmation. Necks of cells producing erythrophil granules pierce female epithelium, this underlain by a layer of circular muscle fibers (7  $\mu$ m thick, holotype) followed by a layer of longitudinal fibers (7  $\mu$ m thick).

# **Remarks**

Among all species of the genus, only *C. taxiarcha* (Marcus, 1951) resembles *C. piguaiatui* in the three-color striped pattern of the dorsum composed of white, yellow, and black

colors. However, in *C. taxiarcha*, the median stripe is white (vs. yellowish in *C. piguaiatui*). Regarding the copulatory apparatus, all species in the genus possess a female atrium as long as the male atrium, with minor variations, whereas in *C. piguaiatui* it is 2.5 times longer. The molecular delimitation methods all clearly point to *C. piguaiatui* being a species differentiated from the rest of species molecularly analysed in the present study.

***Cratera imbir* sp. nov., Araujo, Carbayo, Riutort & Álvarez-Presas**

urn:lsid:zoobank.org:act:CC5B22EB-9E7C-490F-A6FF-03757BA03C26

**Etymology.** The name *imbiri* refers to Vila de São Matheus do Imbiri, former name of Campos do Jordão, type locality of the species.

**Type locality.** Parque Estadual Campos do Jordão, Campos do Jordão, State of São Paulo, Brazil.

**Distribution.** Type locality only.

**Material studied.** Holotype F5512 (MZUSP PL 2155): Parque Estadual Campos do Jordão, Campos do Jordão, State of São Paulo, Brazil (-22.68878, -45.48068). F. Carbayo et al., 15 November 2012. Horizontal sections of a behind cephalic extremity slides; transverse sections of pre-pharyngeal on 9 slides; sagittal sections of pharynx on 13 slides; sagittal sections of copulatory apparatus on 9 slides.

# **Diagnosis**


Species of *Cratera* 26 mm long preserved; dorsal median stripe sulfur yellow bordered on either side by a khaki grey band; body margins cream; in anterior 1/4th of the body, this pattern covered with a color gradient of coral red; eyes marginal; pharynx cylindrical, with


dorsal insertion posteriorly shifted at the equivalent of 20% the length of pharynx; pharyngeal pouch 600 µm anterior to prostatic vesicle; paired portion of the prostatic vesicle with 1/3th of total length of this organ; epithelium of penis papilla underlain by a layer of circular muscle fibers ~~only~~; female atrium 2.5 times longer than male atrium; female atrium narrows gradually towards its posterior section; common glandular ovovitelline duct long.

# **Description**

When creeping, body 38 mm long and 2.5 mm wide. Preserved 26 mm and 4 mm, respectively. Body margins parallel along most of its length. Extremities of the body rounded. The dorsum slightly convex, ventral side flattened. Creeping sole, 94% of body width at the pharyngeal region. Mouth at a distance from anterior extremity equal to 70% of body length; gonopore, 78%.

Dorsal color with a sulfur yellow median stripe, 14% of the body width, this bordered on either side by a khaki grey band, 34% of the body width. Body margins (9% of body width) cream (Fig. 12A). In anterior 1/4th of body, this pattern covered with a gradient ~~color~~ of coral red. Ventral side coral red along anterior 1/4th, and cream colored ~~behind~~ (Fig. 12B).

 Eyes of one pigmented cup with 25 µm in diameter. No clear halos around eyes were seen. Eyes contour the anterior extremity in a single row and extend marginally ~~until~~ posterior

extremity.  Anterior extremity of body with 3mm long not available (used for DNA extraction).

Sensory pits, 20 µm deep, as a uniserial ventro-lateral row in along a body portion initiating 3

mm behind anterior tip of the body and  ending backwards 3.7 mm. Necks of cell glands

producing erythrophil granules pierce dorsal and ventral epithelium in prepharyngeal region.

~~Besides~~, rhabditogen cells discharge their content through dorsal epithelium. Glandular margin

constituted of abundant glands producing erythrophil granules.

Cutaneous musculature of a subepithelial circular layer, followed by two diagonals with decussate fibers, and then a strongly developed longitudinal, 35  $\mu\text{m}$  thick dorsally and 30  $\mu\text{m}$  thick ventrally. Thickness of cutaneous muscle, 11.3% of body height in the pre-pharyngeal region.

Three parenchymal muscle layers are present throughout the body: a dorsal layer of diagonal decussate fibers (10  $\mu\text{m}$  thick), a transverse suprainestinal layer (20  $\mu\text{m}$ ), and a transverse subintestinal one (20  $\mu\text{m}$ ).

Central nervous system as a ventral nerve plate. Cerebral ganglia not discerned.

Mouth located at the end of the anterior half of pharyngeal pouch (Fig. 12C). Pharynx cylindrical, with dorsal insertion posterior to the ventral at the equivalent of 7% of pharyngeal length. Esophagus length, 20% of pharyngeal length. Outer pharyngeal epithelium underlain by a one-fiber-thick layer of longitudinal muscle fibers followed by a layer of circular fibers (5  $\mu\text{m}$  thick); inner pharyngeal epithelium underlain by a layer of circular muscle fibers (60-100  $\mu\text{m}$ ), followed by a layer of longitudinal fibers (8  $\mu\text{m}$ ). Pharyngeal pouch 80  $\mu\text{m}$  anterior to prostatic vesicle.

Testes dorsal, located under the suprainestinal transverse muscle layer, partially placed between the intestinal diverticula. The testes extend from 200  $\mu\text{m}$  behind the level of the ovaries to 1 mm anterior to the root of pharynx. Sperm ducts very narrowed at the point of communication with the respective branch of prostatic vesicle. Paired portion of this vesicle with ca. 1/3rd of the total length of the organ. Prostatic vesicle extrabulbar, running postero-dorsally until anterior region of penis bulb. Vesicle lined with a ciliated epithelium, this pierced by necks of cells producing fine erythrophil granules. A 50- $\mu\text{m}$ -thick circular muscle surround the vesicle. Inside the penis papilla, vesicle communicates with the horizontal, sinuous ejaculatory duct. This

duct is dilatated distally at the tip of the penis papilla the equivalent of 2/5th of length of penis papilla. Ejaculatory duct lined with a cuboidal, ciliated epithelium, its cilia being as long as cell height, i.e., 10  $\mu$ m. ~~This epithelium~~ surrounded by a 5- $\mu$ m-thick layer of circular muscle fibers.

Penis papilla short, horizontally ~~placed, cylindrical~~, with rounded tip; it is shorter than male atrium (Fig. 13A-C). Male atrium as long as 1.2 its height, with smooth folds. A large, transverse, annular fold strongly narrows communication with female atrium (Fig. 13A, C). Penis papilla and male atrium clothed with a cuboidal-to-columnar, non-ciliated epithelium; the subapical portion of its cells is xanthophil. Papillar epithelium pierced by necks two types of cells producing granules, one erythrophil, another weakly basophil. Additionally, cells with gross necks (6  $\mu$ m in diameter) and erythrophil amorphous appearance are located immediately under the epithelium. Epithelium of penis papilla and that of male atrium underlain by a 6- $\mu$ m-thick layer of circular muscle fibers.

Ovaries ellipsoid, ~~with 100  $\mu$ m anteroposteriorly~~ (Fig. 13D), located immediately above the ventral nerve plate, at a distance from anterior tip equivalent to 21% of body length. Ovovitelline ducts arise from dorso-~~external side~~ of ovaries, subsequently run backwards above the ventral nerve plate. ~~They~~ ascend laterally to the female atrium to unite the common glandular ovovitelline duct ~~dorsally to mid female atrium~~ (Fig. 13A). The distal half ascending portion of the ducts receives shell glands. ~~0.9-mm-long~~ common glandular ovovitelline duct (47% of the length of female atrium) communicates with the female genital canal, this a projection of the postero-dorsal portion of the female atrium directed forwards and dorsally. Female atrium with 3.2x the length of male atrium. Posterior third of female atrium with lateral folds narrowing its lumen. Female atrium lined with a non-ciliated, 20  $\mu$ m tall epithelium along anterior 3/4 of its length; tissue of posterior portion is damaged. Gland cells producing erythrophil granules

discharge their secretion into female atrium. It seems to be underlain by two muscle layers, but sections are suboptimal in quality.

# **Remarks**

This small species displays a color pattern that cannot be confounded with any of its congeners. Regarding the internal morphology, only *C. piguaiatui* resembles *C. imbiri* in that both species have an uncommonly long female atrium, at least 2.5 times longer than the male one. Indeed, *C. piguaiatui* and *C. imbiri* are very alike each other in the general aspect of the copulatory apparatus. They distinguished from each other in a set of minor anatomical details: (a) the pharyngeal pouch is 600 µm anterior to the prostatic vesicle (vs. practically leveled with the prostatic vesicle in *C. imbiri*); (b) dorsal insertion of the pharynx is posteriorly shifted at the equivalent of 20% the length of pharynx (vs. 7% in *C. imbiri*); (c) paired portion of the prostatic vesicle is 1/3th of total length of this organ in *C. piguaiatui* (vs. half in *C. piguaiatui*); (d) epithelium of penis papilla is underlain by a layer of circular muscle fibers followed by a layer of longitudinal one in *C. piguaiatui* (vs. only a layer of circular muscle in *C. imbiri*); and (e) the female atrium narrows abruptly towards its posterior section in *C. piguaiatui* (vs. gradually in *C. imbiri*). The molecular based phylogeny shows these two species as very close genetically, nonetheless, the molecular delimitation shows them to be two clearly distinct species which reinforces the minor anatomical differences found to be in fact species specific.

***Cratera paraitinga* sp. nov., Araujo, Carbayo, Riutort & Álvarez-Presas**

urn:lsid:zoobank.org:act:7B3F43A7-2794-42F4-B99F-B8C062F972CF

**Etymology.** The name *paraitinga* refers to São José do Paraitinga, former name of Salesópolis,

795 type locality of the species.

796 **Type locality.** Estação Biológica de Boraceia, Salesópolis, São Paulo State, Brazil.

797 **Distribution.** Type locality only.

798 **Material studied.** Holotype F5769 (MZUSP PL 2157): Estação Biológica de Boraceia,  
799 Salesópolis, São Paulo State, Brazil (-23.65413, -45.88884). F. Carbayo et al., 20 April 2013.

800 Transverse sections of cephalic extremity on 19 slides; horizontal sections of a portion  
801 immediately behind on 71 slides; transverse sections of pre-pharyngeal on 22 slides; sagittal  
802 sections of the pharynx on 33 slides; sagittal sections of copulatory apparatus on 60 slides.

803 Paratype F5745 (MZUSP PL 2156): Ibidem. Transverse sections of cephalic extremity on 11  
804 slides; horizontal sections of an immediately behind on 23 slides; transverse sections of pre-  
805 pharyngeal on 7 slides; sagittal sections of pharynx and copulatory apparatus on 12 slides.

# 806 **Diagnosis**

807 Species of *Cratera* 76 mm long preserved; dorsal melon yellow median stripe, bordered  
808 on either side by a jet black stripe external to each a marginal traffic white stripe; body margins  
809 jet black; eyes marginal; anterior 1/6th of the body colored with a gradient of carmine red;  
810 pharynx bell-shaped; pharyngeal pouch leveled with prostatic vesicle; distal dilatation of  
811 ejaculatory duct relatively large; penis papilla as long as male atrium; female atrium 2.4 times  
812 longer than the male atrium; common glandular ovovitelline duct long.

# 813 **Description**

814 Preserved holotype is 76 mm in length and 7 mm in width. Paratype (incompletely  
815 mature), 27 and mm 4, respectively. The body is slightly lanceolate, with maximum width at the  
816 level of the pharynx. Anterior to it, body thinner gradually to the rounded extremity; near  
817 posterior extremity thinner more abruptly to the pointed tip. Dorsum convex, ventral side



flattened. Creeping sole, 95% of body width at pre-pharyngeal region. Mouth at a distance from anterior extremity equal to 63% of body length; gonopore, 83% (holotype).

Dorsum with ~~an orange~~ luminous median stripe, 40% of the body width, ~~this~~ bordered ~~on~~ ~~either side~~ by a jet-black stripe (14.5%), ~~external which~~ a white band (11%); body margin (4.5%) jet black (Fig. 14A-B). Body ~~sides~~ of anterior 1/5th of the body colored with a gradient of carmine red. Ventrally, body ~~sides~~ of anterior 1/6th orange brown, grey white behind (Fig. 14C).

Each eye is formed by a single pigmented cup with 25 µm in diameter. No clear halos around eyes were ~~seen~~. Eyes contour the anterior extremity in a single row and ~~extend~~ marginally until posterior tip. Sensory pits, 15 µm deep, as a uniserial ventro-lateral row, **from**

**anterior extremity through a body length** at least equal to 15% of body length (holotype). Necks of two types of cell glands, producing xanthophil and erythrophil granules, respectively, pierce prepharyngeal region dorsally and ventrally. ~~Besides~~, rhabditogen cells discharge their secretion through dorsal ~~epithelium~~. Conspicuous glandular margin ~~constituted of~~ abundant glands producing xanthophil granules (Fig. 15A).

Cutaneous musculature of a subepithelial circular layer, followed by two diagonals with decussate fibers, and then a strongly developed longitudinal, 35-40 µm thick (paratype and holotype, respectively) dorsally and 40-45 µm thick ventrally (holotype and paratype, respectively). Thickness of cutaneous ~~muscle~~ ranges from 6.6% (holotype) to 10.7% (paratype) to body height in the pre-pharyngeal region.

Three parenchymal muscle layers present throughout the body, all constituted by fibers relatively densely packed: a dorsal layer of diagonal decussate fibers (10 µm thick, holotype), a suprainestinal layer of transverse muscle fibers (40 µm), and a transverse subintestinal one (40 µm). Dorso-ventral fibers abundant between intestinal branches.

Central nervous system as a ventral nerve plate. Clearly evident cerebral ganglia were not found.

Mouth located in the end of the anterior half of pharyngeal pouch (Fig. 15B). Pharynx bell-shaped, with dorsal insertion posterior to the ventral at the equivalent of 40% of pharyngeal length. Esophagus length, 20% of pharyngeal length (holotype and paratype). Outer pharyngeal epithelium underlain by a one-fiber-thick layer (4  $\mu$ m) of longitudinal muscle fibers followed by a layer of circular fibers (6  $\mu$ m); inner pharyngeal epithelium underlain by a layer (50-100  $\mu$ m) of circular fibers, followed by a layer (20  $\mu$ m) of longitudinal fibers (holotype). Pharyngeal pouch at 80  $\mu$ m from prostatic vesicle (holotype), i.e., 0.001% of body length.

Testes dorsal, located under the suprintestinal muscle layer, partially placed between the intestinal diverticula (Fig. 15A). ~~These~~ testes extend from shortly behind the level of the ovaries to nearly 3 mm anterior to root of pharynx (holotype). Sperm ducts communicate with the respective lateral diverticulum of the prostatic vesicle. ~~This vesicle extrabulbar, elongate, with anterior 1/4th of its length branched.~~ Vesicle runs posteriorly and upwards until anterior region of penis bulb. Vesicle is lined with a ciliated epithelium, which is pierced by numerous necks of cells producing fine erythrophil granules. A 15- $\mu$ m-thick net of muscle fibers surround the vesicle. Inside the penis papilla, vesicle communicates with a straight ejaculatory duct traversing penis papilla at the tip of which dilates to a conspicuous cavity with half of penis papilla length (Fig. 15C, 16A-B). ~~Epithelium of this duct~~ surrounded by a 5- $\mu$ m-thick layer of circular muscle fibers along most of its length, and of circular and longitudinal fibers in its dilated portion.

Penis papilla conical, with dorsal insertion slightly posterior to the ventral one; it is as long as male atrium (Fig. 15C, 16A). Male atrium as long as 1.4x its height, slightly folded. Penis papilla and male atrium clothed with a cuboidal, non-ciliated epithelium, which is pierced

864 by necks of cells producing erythrophil granules. Quality of stain did not provide further details.  
865 Epithelium of penis papilla and that of male atrium underlain by a 3- $\mu$ m-thick layer of circular  
866 muscle fibers, followed by a 2- $\mu$ m-thick layer of longitudinal fibers.

867 ~~Ovaries elongated, ovoid, with 300  $\mu$ m anteroposteriorly.~~ They are located immediately  
868 above the ventral nerve plate, at a distance from anterior tip equivalent to 25% of body length  
869 (holotype). Ovovitelline ducts arise from dorso-lateral side of the ovaries and run backwards  
870 above the ventral nerve plate. ~~They ascend laterally to the female atrium to unite the common~~  
871 ~~glandular ovovitelline duct dorsally to female atrium~~ (Fig. 15C). Distal ascending portion of the  
872 ~~ducts receives~~ shell glands. The long common glandular ovovitelline duct (0.9 mm, ie., 1/3th of  
873 the length of female atrium) communicates with female genital canal, the latter being a  
874 projection of posterior portion of female atrium that ~~runs forwards and dorsally~~ (Fig. 15C, 16A-  
875 C). Female atrium long and funnel-shaped, compressed laterally. Anterior portion of female  
876 atrium narrower. Female atrium with 2.4 times the length of male atrium, and lined with non-  
877 ciliated epithelium, 40  $\mu$ m tall and with multilayered aspect in its posteriormost 1/4th; otherwise,  
878 20  $\mu$ m tall and cuboidal-to-columnar. Necks of cells producing erythrophil granules pierce  
879 female epithelium, this underlain by a layer of circular muscle fibers (10  $\mu$ m thick, holotype)  
880 followed by a layer of longitudinal fibers (10  $\mu$ m thick).

# 881 **Remarks**

882 Among all species of the genus, *C. taxiarcha* and *C. piguaiatui* resemble *C. paraitinga* in  
883 the general color pattern of the dorsum consisting of longitudinal stripes with black, white and  
884 yellow color. However, the median stripe in *C. taxiarcha* is white (vs. yellowish in *C.*  
885 *paraitinga*). *Cratera piguaiatui*, very similar to *C. paraitinga* in the color pattern, differs from it  
886 in the width of the yellowish midstripe (28% of body width in *C. piguaiatui* vs. 40% in *C.*

*paraitinga*).

Regarding the copulatory apparatus, only *C. piguaiatui* and *C. imbiru* resemble *C. paraitinga* in the relatively long female atrium when compared with the male one. However, the two species differ from *C. paraitinga* in minor details: (a) the dilatation of the ejaculatory duct is relatively small in *C. piguaiatui* (vs. relatively large in *C. paraitinga*); (b) the pharyngeal pouch is 0.6 mm anterior to the prostatic vesicle in *C. piguaiatui* (vs. practically leveled in *C. paraitinga*); (c) the penis papilla is shorter than the male atrium in *C. piguaiatui* and *C. imbiru* (vs. as long as the male atrium in *C. paraitinga*).

The molecular analyses show these three species, *C. piguaiatui*, *C. imbiru* and *C. paraitinga*, to constitute a monophyletic group, which will explain their morphological similarities commented above and could also raise some doubt on their identity as different species. However, the discovery methods of species delimitation, only with the exception of the mPTP method, show the three as independent species. In the case of the validation method (BPP) the significance of the separation of *C. imbiru* and *C. paraitinga* is only highly supported by the models implying a small ancestral size, while the support is slightly lower if we consider ancestral population was large. It could be interpreted from our results that ancestral populations may not have been very large, although, of course, the current situation may be a consequence of the destruction of their habitat or a lack of sampling, since some areas have been explored very intensively and others are still pending sampling. Putting together all the evidence, molecular and morphology reinforce one another and give more weight to the small morphological differences found to be indicators of the different lineages having become different species.

## Discussion

Carbayo et al. (2013) proposed the first phylogenetic framework of Geoplaninae. That phylogeny was inferred from one mitochondrial region (COI) and three nuclear ones (18S, 28S rDNA and EF) of 68 species, eight of them representing *Cratera* lineages (plus one immature representative). At that time, only three species of *Cratera* were known (*C. crioula*, *C. pseudovaginuloides* and *C. tamoia*). Later, three of the undescribed species considered in that study were formally described (*C. cuarassu*; *C. picuia* Lago-Barcia & Carbayo, 2018, *C. arucuia* Lago-Barcia & Carbayo, 2018). Two species included in the Carbayo et al (2013) phylogeny that had remained morphologically unstudied, are described in the present work, namely *C. piguaiassu* and *C. piguaiatui*.


In the present study, three new species (*C. imbiru*, *C. paraitinga*, *C. piguaiaboja*) are also included for the first time. The phylogenetic relationships between all these 11 species have been examined here through comparative analysis of six concatenated DNA regions (two mitochondrial fragments and four nuclear).

Without taking into consideration differences in representativeness, the topology of our phylogeny matches that of Carbayo et al (2013), except for the position of *C. tamoia* and *C. crioula*. In the phylogeny from 2013, *C. tamoia* is sister of the remaining species of an in-group including *C. crioula*, whereas in the present phylogeny, *C. crioula* + *C. piguaiassu* is the sister clade to the remaining members of the in-group, which includes *C. tamoia*. This is a relevant result, due to a difference in taxon sampling. As more species are included in the present study, relationships are resolved that could not be observed in the phylogenies of 2013, with a smaller representation of species of *Cratera*. Lago-Barcia & Carbayo (2018) discussed the evolution of some morphological attributes within *Cratera* by analyzing them against the phylogeny of Carbayo et al. (2013). They considered only the five species whose anatomy was known, namely

*C. arucuia*, *C. crioula*, *C. cuarassu*, *C. picuia*, and *C. pseudovaginuloides*. They interpreted that the distal widening of the ejaculatory duct originated in the common ancestor of all *Cratera* members and was secondarily lost in the last common ancestor of *C. tamoia*, *C. crioula*, and *C. arucuia*. For this feature as well as other characters (roof of the male atrium pierced by necks of numerous cyanophil glands; prostatic vesicle dorsally located; 900° rotation of the penis papilla), they concluded that "diagnostic character states of the genus can be lost or modified within recently evolved in-groups of *Cratera*, hence puzzling species classification" (Lago-Barcia & Carbayo, 2018).

In the light of this new phylogenetic framework, loss of the widening of distal section of the ejaculatory duct apparently evolved independently in two lineages, thus giving rise to the condition in *C. crioula*, and that in *C. picuia* and *C. arucuia*. However, this new framework does not invalidate the above-quoted conclusion of Lago-Barcia & Carbayo. Moreover, our data corroborates their conclusion as demonstrated in the following five selected examples. (i) The position of the prostatic vesicle, either internal to the penis bulb or external to it, appears to have independently evolved from an external to an internal position only in *C. tamoia* and *C. picuia*. An equally parsimonious interpretation would be that the internal position of the prostatic vesicle would have evolved in the common ancestor of *C. tamoia* + *C. arucuia* + *C. picuia* and that this condition would have reversed in *C. arucuia*. (ii) In similar vein, a penis papilla longer than the male atrium may have been gained in the common ancestor of *C. piguaiaboja*, *C. pseudovaginuloides*, *C. crioula*, *C. piguaiassu*, *C. picuia*, *C. arucuia* and *C. tamoia*, while this condition would independently secondarily have been lost in *C. piguaiaboja* and *C. tamoia*. (iii) In *C. picuia* and *C. piguaiaboja*, the dorsal surface of the male atrium is traversed by a mass of necks of cells producing cyanophil granules. This situation is best explained as two independent

~~gain events~~. (iv) The most parsimonious explanation for the very reduced or even absence of the common glandular ovovitelline duct in *C. picuia*, *C. piguaiassu* and *C. piguaiabaja* is independent loss in each of these species, none of which shares a sister-group relationship.

In ~~the~~  ~~this~~ trend, the relatively long female atrium, in comparison with the male atrium appears to be homologous in all members of *Cratera*. The female atrium is usually as long as the male one. However, in *C. piguaiatui*, *C. imbiru*, and *C. paraitinga*, the female atrium is >2.4 times longer than the male one. These three species constitute a monophyletic group and most probably this character state evolved in the common ancestor of these species. These three species are similar to each other, not only in this trait, but also in the traditional characteristics used in the classification of Geoplaninae. For this reason, our molecular approach in the species delimitation proved to be essential in their discovery as independent lineages.

The causes underlying the evolutionary differences between the copulatory organs in land triclads remain unclear. Absence of relevant apomorphies in other related groups, such as the freshwater planarian genus *Girardia* (Dugesiiidae), also complicated assignment of species to the genus (Sluys, Hauser & Wirth, 1997). In the case of land planarians, morphological differences may be related to the fact that each species belongs to a lineage that has evolved independently for a long period, as exemplified by the land planarian *Cephaloflexa bergi* (Graff, 1899) (Geoplaninae), a species that originated about 7 Mya (Álvarez-Presas et al., 2014).

~~As a result of this argument, it rises that~~ *Cratera* land planarians ~~evolved labile~~ features, even those that diagnose the genus, such as the dilatation of the ejaculatory duct. ~~This lability~~ can mislead a natural classification of *Cratera* and its relatives if systematics is solely based on morphology.

An interesting aspect of land planarians is their restricted geographical distribution. Most

species are known from only one or a few localities (unpublished results). In the present study only *Cratera piguaiatui* was found in an additional locality apart from the type locality. Even so, the two localities are only 30 km apart from each other. Although sampling artifacts may underlie such presumably restricted distributions (Sluys, 1999) it is also possible that they reflect actual species distribution. Our data support the latter in the case of *Cratera* because we performed an intensive sampling effort in the four areas that resulted in the distributional ranges reported in this study.

We hypothesize here that *Cratera* species presenting such labile features, being genetically close among them and with very restricted areas of distribution may be the result of relatively recent speciation events linked to the postglacial history of the area. However, thorough studies including NGS data and robust population analyses will be necessary to confirm such hypothesis.

## Conclusions

Molecular-based phylogenies and species delimitation provide hypotheses on species recognition that are independent from the morphology-based approach. Congruence of both approaches allowed us to recognize evolutionarily independent lineages, i.e, species, and to independently evaluate minor morphological differences among the individuals as a signal of diagnostic attributes of a species. Otherwise, most likely we had ranked *C. piguaiatui*, *C. imbir* and *C. paraitinga* under one nominal species.

Moreover, the new molecular markers for species delimitation and phylogenetic inference developed for the first time in the present work have shown to be highly resolute for terrestrial planarians. We have expanded the number of informative molecular markers by



adding two new molecules (Tnuc813 and Nd4toCox1) as a result of the use of new generation molecular tools. This result should not be overlooked, since the availability of molecular markers has always been a limitation in the study of the systematics of these animals.

## Acknowledgements

We are grateful to the COTEC - Instituto Florestal do Estado de São Paulo (Proc. SMA 12.640/2011), Museu de Zoologia (EBBAut.020/2013) and Instituto Chico Mendes de Conservação da Biodiversidade (Proc. 32779-1; 11748-4) for licensing the field work. We also thank Celso Barbieri Junior, Cláudia Olivares, Débora Redivo, Erica Panachuk de Souza, Júlio Pedroni, Leonardo Zerbone, Marcos Santos Silva, Marília Jucá and Welton Araújo (EACH, USP) for assistance during the sampling. Thanks are due to Geison Castro da Silveira, Lucas Beltrami, and Ítalo Silva de Oliveira Souza (EACH, USP) for histological processing. Gema Blasco is thanked for the wet lab support.

## References

**Almeida AL, Marques FPL, Carbayo F. 2019.** 'Endless forms most beautiful': taxonomic revision of the planarian *Geoplana vaginuloides* (Darwin, 1844) and discovery of numerous

1032 congeners (Platyhelminthes: Tricladida). *Zoological Journal of the Linnean Society* 185: 1–65.  
 1033 <https://doi.org/10.1093/zoolinnean/zly022>

1034 **Álvarez-Presas M, Baguña J, Riutort M. 2008.** Molecular phylogeny of land and freshwater  
 1035 planarians (Tricladida, Platyhelminthes): from freshwater to land and back. *Molecular*  
 1036 *Phylogenetics and Evolution* 47: 555–568. <https://doi.org/10.1016/j.ympev.2008.01.032>

1037 **Álvarez-Presas M, Carbayo F, Rozas J, Riutort M. 2011.** Land planarians (Platyhelminthes)  
 1038 as a model organism for fine-scale phylogeographic studies: understanding patterns of  
 1039 biodiversity in the Brazilian Atlantic Forest hotspot. *Journal of Evolutionary Biology* 24: 887–  
 1040 896. <https://doi.org/10.1111/j.1420-9101.2010.02220.x>

1041 **Ayres DL, Darling A, Zwickl DJ, Beerli P, Holder MT, Lewis PO, et al. 2012.** BEAGLE: An  
 1042 application programming interface and high-performance computing library for statistical  
 1043 phylogenetics. *Systematic Biology* 61: 170–173. <https://doi.org/10.1093/sysbio/syr100>

1044 **Bouckaert R, Heled J, Kühnert D, Vaughan T, Wu C-H, Xie D, et al. 2014.** BEAST2: A  
 1045 software platform for Bayesian evolutionary analysis. *PLOS Computational Biology*.  
 1046 <https://doi.org/10.1371/journal.pcbi.1003537>

1047 **Carbayo F, Álvarez-Presas M, Olivares CT, Marques FPL, Froehlich EM, Riutort M.**  
 1048 **2013.** Molecular phylogeny of Geoplaninae (Platyhelminthes) challenges current classification:  
 1049 proposal of taxonomic actions. *Zoologica Scripta* 42: 508–528.  
 1050 <https://doi.org/10.1111/zsc.12019>

1051 **Carbayo F, & Almeida AL. 2015.** Anatomical deviation of male organs of land planarians from  
 1052 Rio de Janeiro, Brazil, with description of two new species of *Cratera* (Platyhelminthes,  
 1053 Tricladida). *Zootaxa* 3931(1): 027-040. <https://doi.org/10.11646/zootaxa.3931.1.2>

- 1054 **Carbayo F, Silva MS, Riutort M, Álvarez-Presas M. 2018.** Rolling into the deep of the land
- 1055 planarian genus *Choeradoplana* (Tricladida, Continenticola, Geoplanidae) taxonomy. *Organisms*
- 1056 *Diversity & Evolution* 18: 187–210. <https://doi.org/10.1007/s13127-017-0352-4>
- 1057 **Carranza S, Giribet G, Ribera C, Baguña J, Riutort M. 1996.** Evidence that Two Types of
- 1058 18s rDNA Coexist in the Genome of *Dugesia (Schmidtea) mediterranea* (Platyhelminthes,
- 1059 Turbellaria, Tricladida). *Molecular Biology and Evolution* 13: 824–832.
- 1060 <https://doi.org/10.1093/oxfordjournals.molbev.a025643>
-  1061 **Cason. 1950.** A rapid one-step Mallory-Heidenhain stain for connective tissue. *Stain Technology*
- 1062 25(4): 225–226. <https://doi.org/10.3109/10520295009110996>
- 1063 **Darriba D, Taboada GL, Doallo R, Posada D. 2012.** jModelTest 2: more models, new
- 1064 heuristics and parallel computing. *Nature Methods* 9: 772. <https://doi.org/10.1038/nmeth.2109>
- 1065 **Froehlich EM. 1955.** Sobre espécies brasileiras do gênero *Geoplana*. *Boletim da Faculdade de*
- 1066 *Filosofia, Ciências e Letras da Universidade de São Paulo, Série Zoologia* 19: 289–369.
- 1067 **Hall TA. 1999.** BioEdit: a user-friendly biological sequence alignment editor and analysis
- 1068 program for Windows 95/98/NT. *Nucleic acids symposium series* 41: 95–98.
- 1069 **Kapli P, Lutteropp S, Zhang J, Kobert K, Pavlidis P, Stamatakis A, et al. 2017.** Multi-rate
- 1070 Poisson tree processes for single-locus species delimitation under maximum likelihood and
- 1071 Markov chain Monte Carlo. *Bioinformatics* 33: 1630–1638.
- 1072 <https://doi.org/10.1093/bioinformatics/btx025>
- 1073 **Katoh K, Rozewicki J, Yamada KD. 2017.** MAFFT online service: multiple sequence
- 1074 alignment, interactive sequence choice and visualization. *Briefings in Bioinformatics* bbx108: 1–
- 1075 7. <https://doi.org/10.1093/bib/bbx108>

1076 **Lago-Barcia D & Carbayo F. 2018.** Taxonomic revision of four species of the Neotropical land  
1077 planarian genera *Cratera* and *Geoplana* (Platyhelminthes, Tricladida) with a description of two  
1078 new species and an emendation of *Cratera*. *Zootaxa* 4500 (4): 517–542.  
1079 <https://doi.org/10.11646/zootaxa.4500.4.3>

1080 **Lanfear R, Frandsen PB, Wright AM, Senfeld T, Calcott B. 2017.** Partitionfinder 2: New  
1081 methods for selecting partitioned models of evolution for molecular and morphological  
1082 phylogenetic analyses. *Molecular Biology and Evolution* 34: 772–773.  
1083 <https://doi.org/10.1093/molbev/msw260>

1084 **Lázaro EM, Sluys R, Pala M, Stocchino GA, Bagnà J, Riutort M. 2009.** Molecular  
1085 barcoding and phylogeography of sexual and asexual freshwater planarians of the genus *Dugesia*  
1086 in the Western Mediterranean (Platyhelminthes, Tricladida, Dugesidae). *Molecular*  
1087 *Phylogenetics and Evolution* 52: 835–845. <https://doi.org/10.1016/j.ympev.2009.04.022>

1088 **Leria L, Vila-Farré M, Álvarez-Presas M, Sánchez-Gracia A, Rozas J, Sluys R, Riutort M.**  
1089 **2020.** Cryptic species delineation in freshwater planarians of the genus *Dugesia*  
1090 (Platyhelminthes, Tricladida): Extreme intraindividual genetic diversity, morphological stasis,  
1091 and karyological variability. *Molecular Phylogenetics and Evolution*, 143: 106496.  
1092 <https://doi.org/10.1016/j.ympev.2019.05.010>

1093 **Marcus E. 1951.** Turbellaria brasileiros (9). *Boletim da Faculdade de Filosofia, Ciências e*  
1094 *Letras da Universidade de São Paulo, Série Zoologia* 16: 1–217.

1095 **Miller MA, Pfeiffer W, Schwartz T. 2010.** Creating the CIPRES Science Gateway for  
1096 Inference of Large Phylogenetic Trees. *Proceedings of the Gateway Computing Environments*  
1097 *Workshop (GCE)*. New Orleans, LA; 1–8. <https://doi.org/10.1109/GCE.2010.5676129>

- 1098 **Minh BQ, Nguyen MAT, Von Haeseler A. 2013.** Ultrafast approximation for phylogenetic  
1099 bootstrap. *Molecular Biology and Evolution* 30: 1188–1195.  
1100 <https://doi.org/10.1093/molbev/mst024>
- 1101 **Negrete L, & Brusa F. 2016.** First report of the genus *Cratera* (Platyhelminthes, Geoplanidae) in  
1102 Argentina, with description of a new species and comments on the species of the genus. *ZooKeys*  
1103 610: 1–12. <https://doi.org/10.3897/zookeys.610.9465>
- 1104 **Nguyen LT, Schmidt HA, Von Haeseler A, Minh BQ. 2015.** IQ-TREE: A fast and effective  
1105 stochastic algorithm for estimating maximum-likelihood phylogenies. *Molecular Biology and*  
1106 *Evolution* 32: 268–274. <https://doi.org/10.1093/molbev/msu300>
- 1107 **Puillandre N, Modica MV, Zhang Y, Sirovich L, Boisselier MC, Cruaud C, et al. 2012a.**  
1108 Large-scale species delimitation method for hyperdiverse groups. *Molecular Ecology* 21: 2671–  
1109 2691. <https://doi.org/10.1111/j.1365-294X.2012.05559.x>
- 1110 **Puillandre N, Lambert A, Brouillet S, Achaz G. 2012b.** ABGD, Automatic Barcode Gap  
1111 Discovery for primary species delimitation. *Molecular Ecology* 21: 1864–1877.  
1112 <https://doi.org/10.1111/j.1365-294X.2011.05239.x>
- 1113 **Ronquist F, Teslenko M, Van Der Mark P, Ayres DL, Darling A, Höhna S, et al. 2012.**  
1114 MrBayes 3.2: Efficient Bayesian Phylogenetic Inference and Model Choice Across a Large  
1115 Model Space. *Systematic Biology* 61: 539–542. <https://doi.org/10.1093/sysbio/sys029>
- 1116 **Riester A. 1938.** Beiträge zur Geoplaniden-Fauna Brasiliens. *Abhandlungen der*  
1117 *Senckenbergischen Naturforschenden Gesellschaft* 441: 1–88.
- 1118 **Rossi I, Amaral SV, Ribeiro GG, Cauduro GP, Fick I, Valiati VH, Leal-Zanchet AM. 2016.**  
1119 Two new Geoplaninae species (Platyhelminthes: Continenticola) from Southern Brazil based on

1120 an integrative taxonomic approach. *Journal of Natural History* 50(13-14): 787-815.  
 1121 <https://doi.org/10.1080/00222933.2015.1084057>

1122 **Rossi I & Leal-Zanchet A. 2017.** Three new species of *Cratera* Carbayo et al., 2013 from  
 1123 *Araucaria* forests with a key to species of the genus (Platyhelminthes, Continenticola). *ZooKeys*  
 1124 643: 1–32. <https://doi.org/10.3897/zookeys.643.11093>

1125 **Sluys R, Hauser J, Wirth QJ. 1997.** Deviation from the Groundplan: a unique new species of  
 1126 freshwater planarian from South Brazil (Platyhelminthes, Tricladida, Paludicola). *Journal of*  
 1127 *Zoology* 241(3): 593-601. <https://doi.org/10.1111/j.1469-7998.1997.tb04851.x>

1128 **Sluys R. 1999.** Global diversity of land planarians (Platyhelminthes, Tricladida, Terricola): a  
 1129 new indicator-taxon in biodiversity and conservation studies. *Biodiversity & Conservation* 8(12):  
 1130 1663-1681. <https://doi.org/10.1023/A:1008994925673>

1131 **Sluys R, Mateos E, Riutort M, Alvarez-Presas M. 2016.** Towards a comprehensive,  
 1132 integrative analysis of the diversity of European microplaninid land flatworms (Platyhelminthes,  
 1133 Tricladida, Microplaninae), with the description of two peculiar new species. *Systematics and*  
 1134 *Biodiversity* 14(1): 9-31. <https://doi.org/10.1080/14772000.2015.1103323>

1135 **Sluys R. 2016.** Invasion of the flatworms. *American Scientist* 104(5): 288-295.  
 1136 <https://doi.org/10.1511/2016.122.288>

1137 **Talavera G & Castresana J. 2007.** Improvement of Phylogenies after Removing Divergent and  
 1138 Ambiguously Aligned Blocks from Protein Sequence Alignments. *Systematic Biology* 56: 564–  
 1139 577. <https://doi.org/10.1080/10635150701472164>

1140 **Yang Z & Rannala B. 2010.** Bayesian species delimitation using multilocus sequence data.  
 1141 *Proceedings of the National Academy of Sciences* 107: 9264–9269.  
 1142 <https://doi.org/10.1073/pnas.0913022107>

- 1143 **Yang Z & Rannala B. 2014.** Unguided species delimitation using DNA sequence data from
- 1144 multiple loci. *Molecular Biology and Evolution* 31: 3125–3135.
- 1145 <https://doi.org/10.1093/molbev/msu279>
- 1146 **Yang Z. 2015.** The BPP program for species tree estimation and species delimitation. *Current*
- 1147 *Zoology* 61: 854–865. <https://doi.org/10.1093/czoolo/61.5.854>

# Figure 1

Map showing the sampling sites.

Records of the five species of *Cratera* described in this paper.



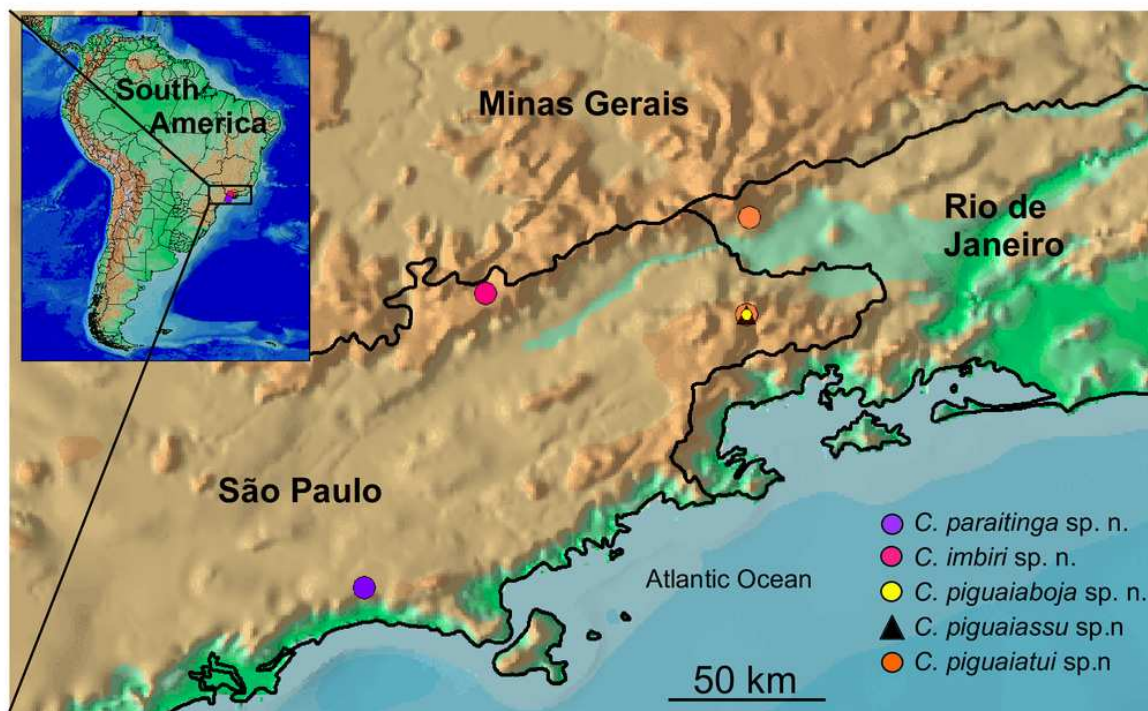


Figure 1



# Figure 3

Results of BPP molecular species delimitation.

Results of BPP represented in the species tree estimated with \*BEAST for the genus *Cratera*. Colored squares of the nodes represent PP values for each of the applied models (M1, left up, M2, right up, M3, left down, M4, right down). Colors correspond to PP values: 1 (blue),  $> 0.95$  (orange), or  $< 0.95$  (green). Nomenclature of Primary Species Hypothesis (PSH) is shown at the terminals of the branches. On the right, green letters indicate the Secondary Species Hypothesis validated by BPP. The images correspond to the new species. The scale bar represents substitutions per site.

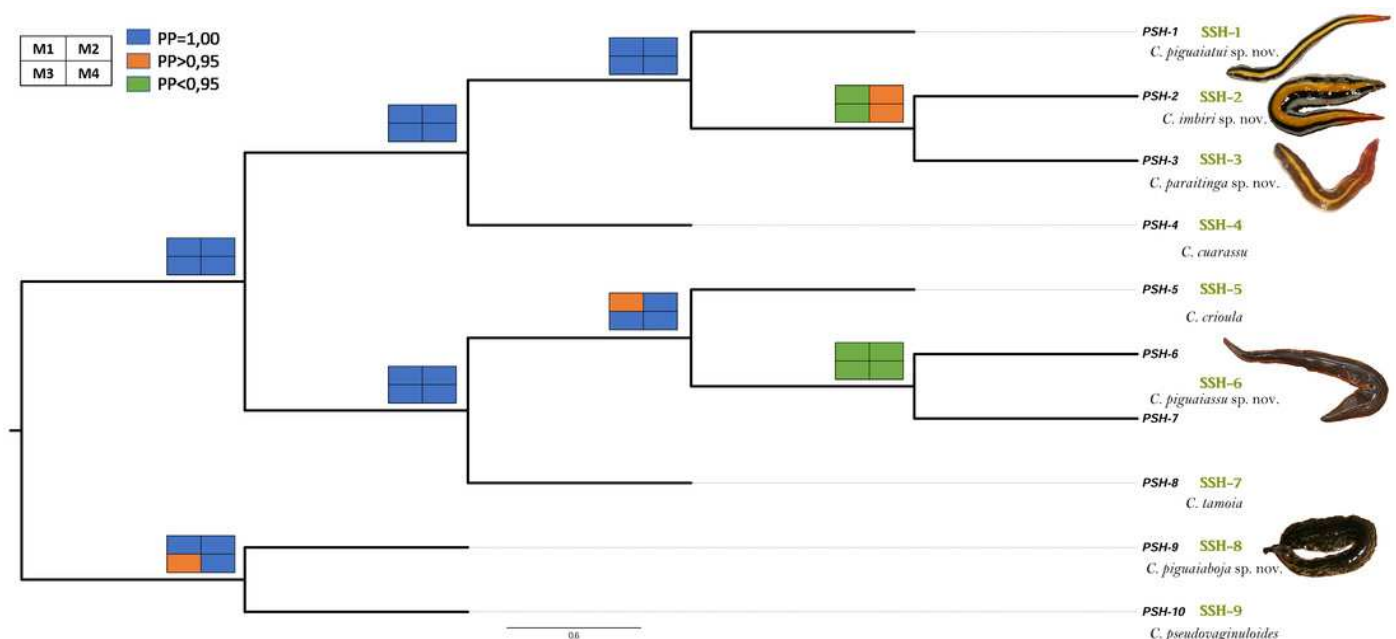


# Figure 4

*Cratera piguaiassu* sp. n. morphological characters.

*Cratera piguaiassu* sp. n. (A): dorsal and ventral (inset) views of living paratype F2807. Scale bar not available. (B): dorsal and ventral (inset) views of living paratype F2821. Scale bar not available. (C): photomicrograph of a sagittal section of the pharynx of holotype. (D): photomicrograph of a transverse section of pre-pharyngeal region of paratype F2807.

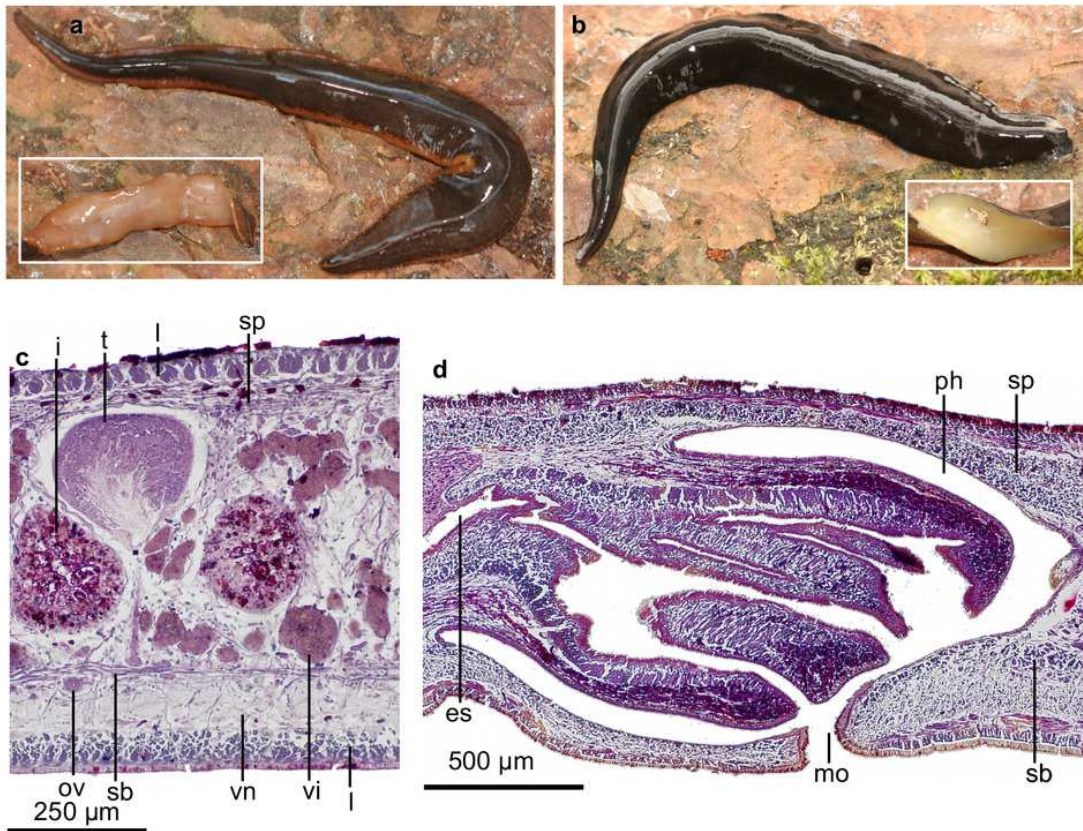


# Figure 5

*Cratera piguaiassu* sp. n. morphological details.

*Cratera piguaiassu* sp. n. (A): diagrammatic representation of the copulatory apparatus of holotype from sagittal sections. (B) photomicrograph of a sagittal section of the copulatory apparatus of holotype. (C): photomicrograph of a sagittal section of the copulatory apparatus of paratype F2821. (D): photomicrograph of a sagittal section of the female atrium of paratype F2025.



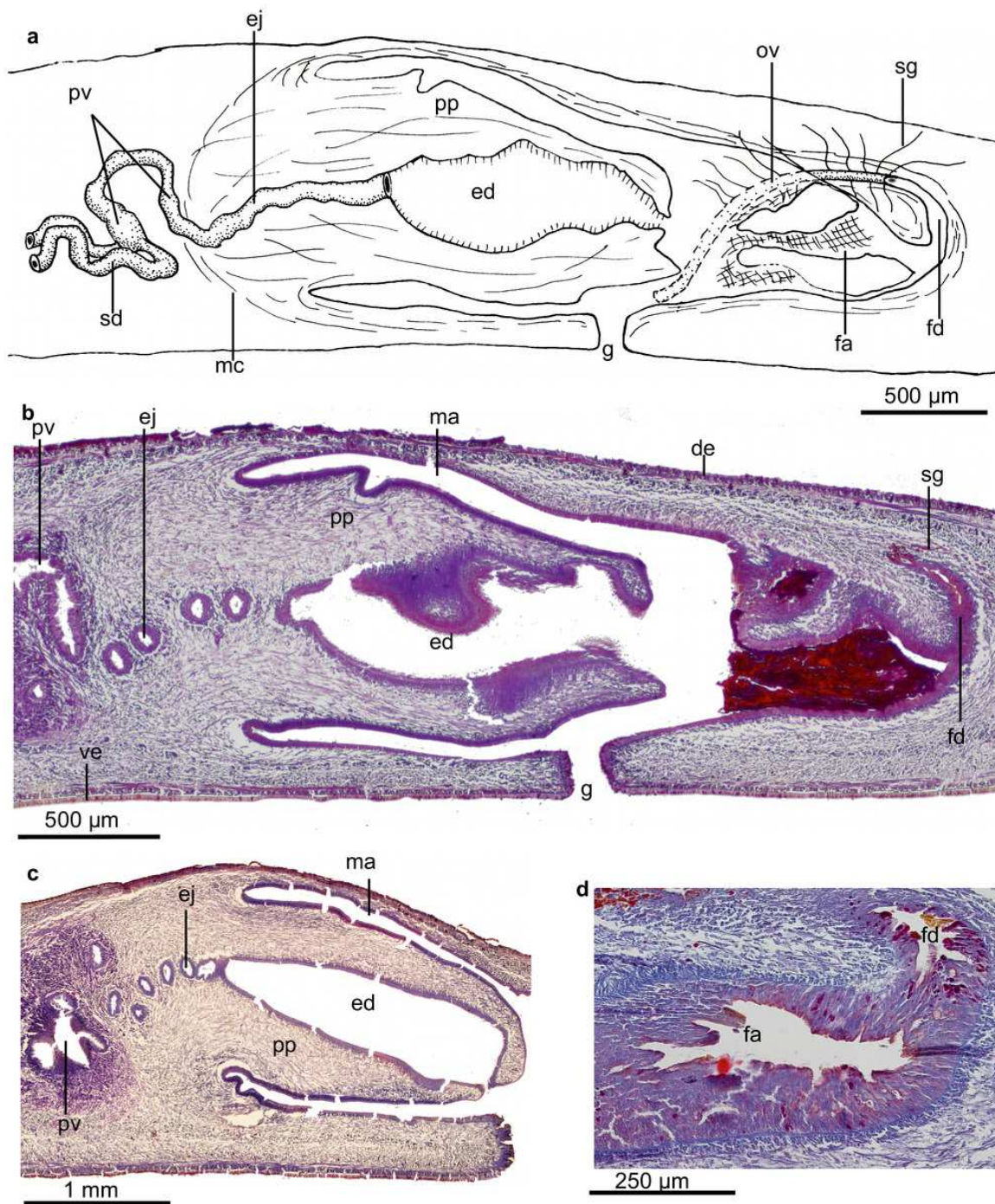


# Figure 6

*Cratera piguaiaboja* ~~sp. n.~~ morphological details.

*Cratera piguaiaboja* ~~sp. n.~~ (A): Living holotype. Scale bar not available. (B): Dorsal view of living paratype. Scale bar not available. (C): dorsal view of holotype preserved on millimeter graph paper after cutting off a piece of the body. (D): dorsal view of the paratype, preserved on millimeter graph paper after cutting off anterior ~~extremity~~ of the body.





# Figure 7

*Cratera piguaiaboja* ~~sp. n.~~ morphological details.

*Cratera piguaiaboja* ~~sp. n.~~ (A): photomicrograph of a transverse section of pre-pharyngeal region of holotype. (B): photomicrograph of a sagittal section of the pharynx of paratype. (C): diagrammatic representation of the copulatory apparatus of paratype from sagittal sections. (D): diagrammatic representation of the copulatory apparatus of holotype from sagittal sections.

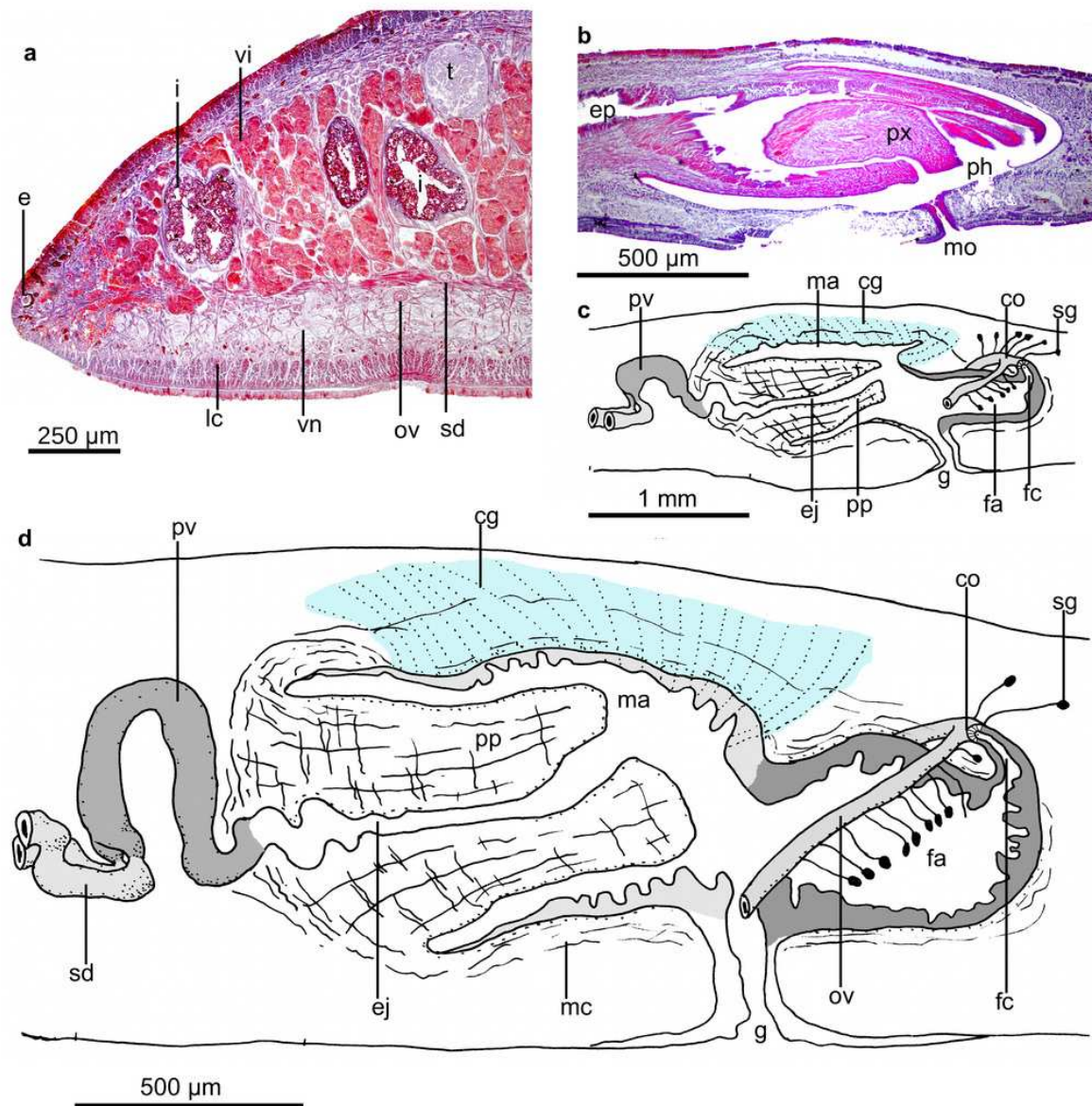


# Figure 8

*Cratera piguaiaboja* ~~sp. n.~~ morphological features.

*Cratera piguaiaboja* ~~sp. n.~~ Photomicrographs of sagittal sections. (A): Copulatory apparatus of paratype. (B): Female atrium of holotype. (C): Female atrium of paratype.



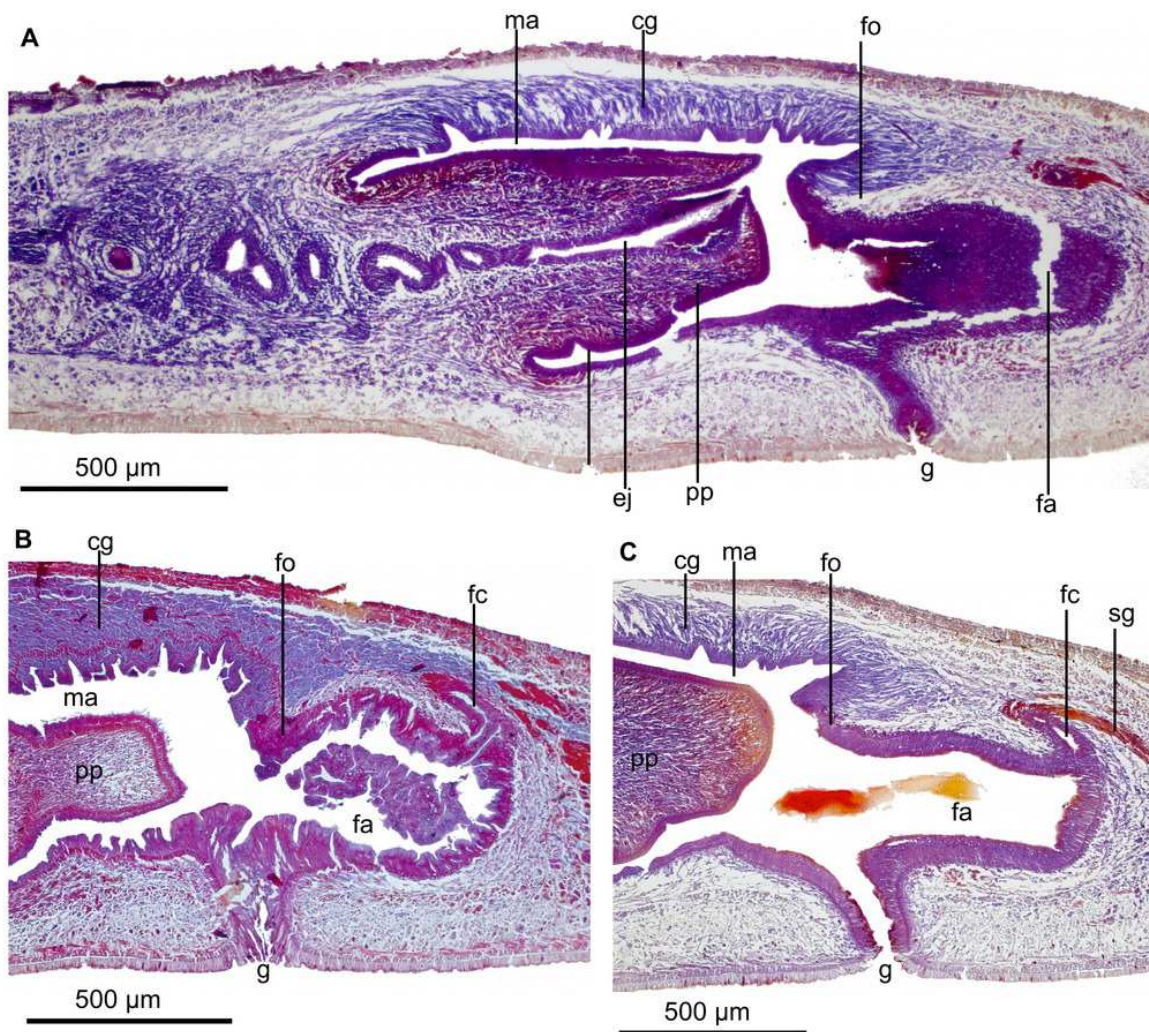


# Figure 9

*Cratera piguaiatui* ~~sp. n.~~ morphological features.

*Cratera piguaiatui* ~~sp. n.~~ (A): Dorsal view of living paratype F5178. (B): Dorsal view of living holotype partially twisted. ~~Scales~~ not available.



Fig. 1

# Figure 10

*Cratera piguaiatui* ~~sp. n.~~ morphological features.

*Cratera piguaiatui* ~~sp. n.~~ (A): photomicrograph of a transverse section of pre-pharyngeal region of holotype. (B): diagrammatic representation of the pharynx of paratype F2054 from sagittal sections.



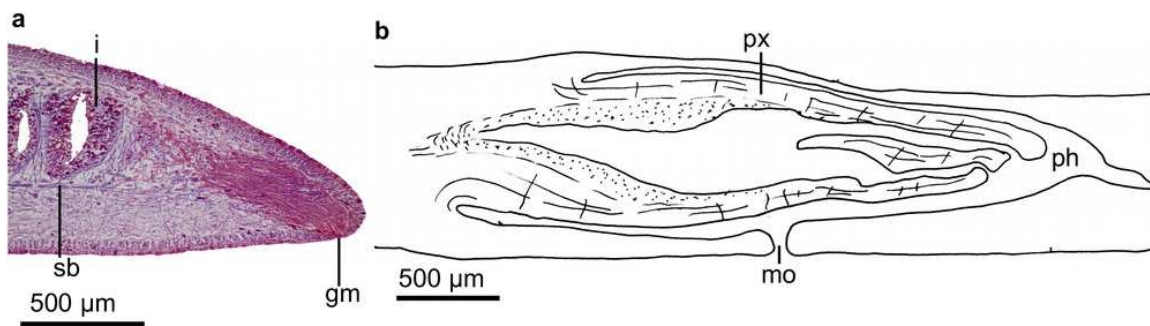


# Figure 11

*Cratera piguaiatui* ~~sp. n.~~ morphological details.

*Cratera piguaiatui* ~~sp. n.~~ Holotype. (A) diagrammatic representation of the copulatory apparatus from sagittal sections. (B): photomicrograph of a sagittal section of copulatory apparatus. (C): photomicrograph of a sagittal section penis papilla.

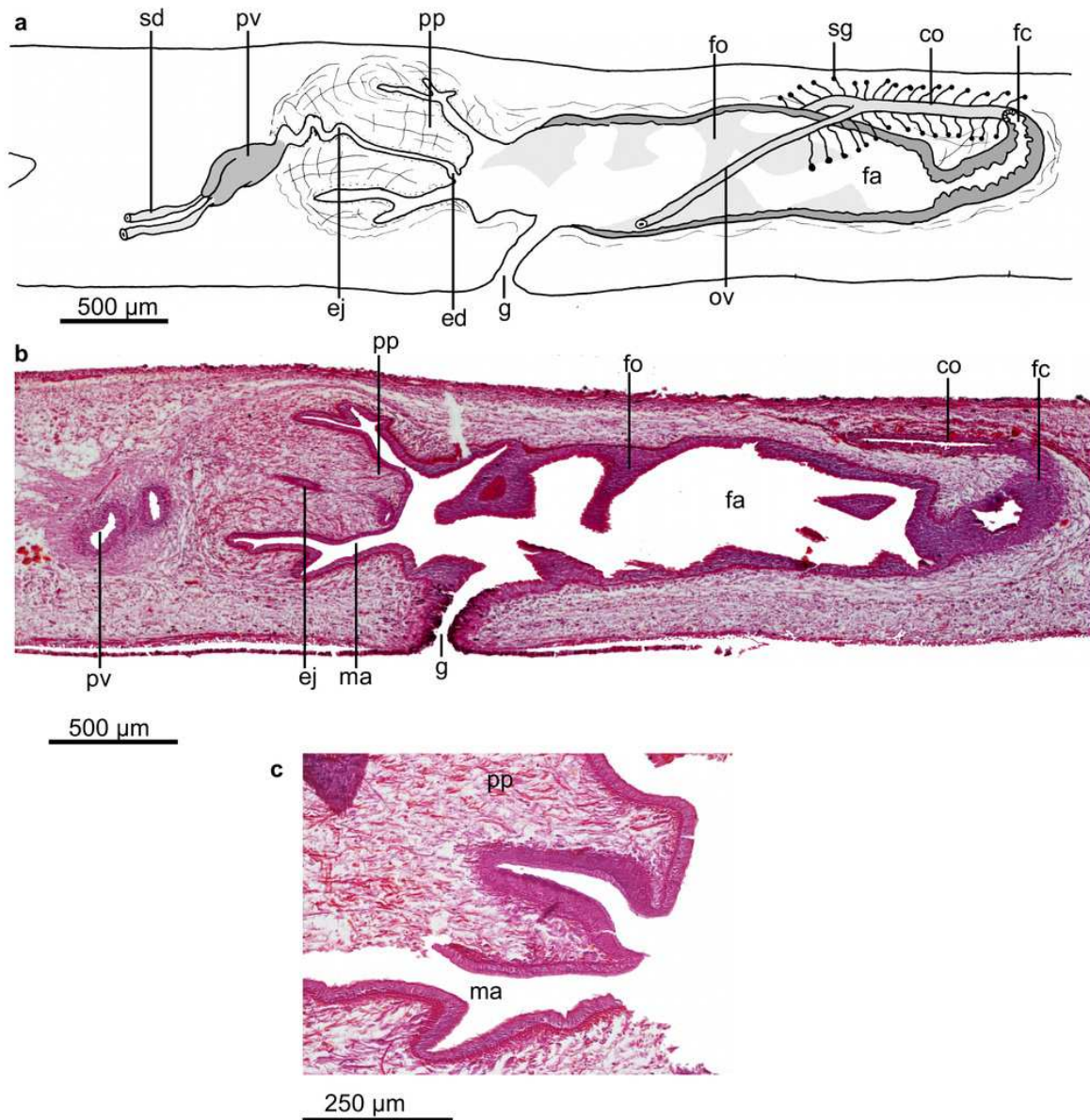


# Figure 12

*Cratera imbiri* ~~sp. n.~~ morphological features.

*Cratera imbiri* ~~sp. n.~~ Holotype (A): Dorsal view of living specimen. Scale bar not available. (B): Ventral view of living specimen. Scale bar not available. (C): photomicrograph of a sagittal section of pharynx.

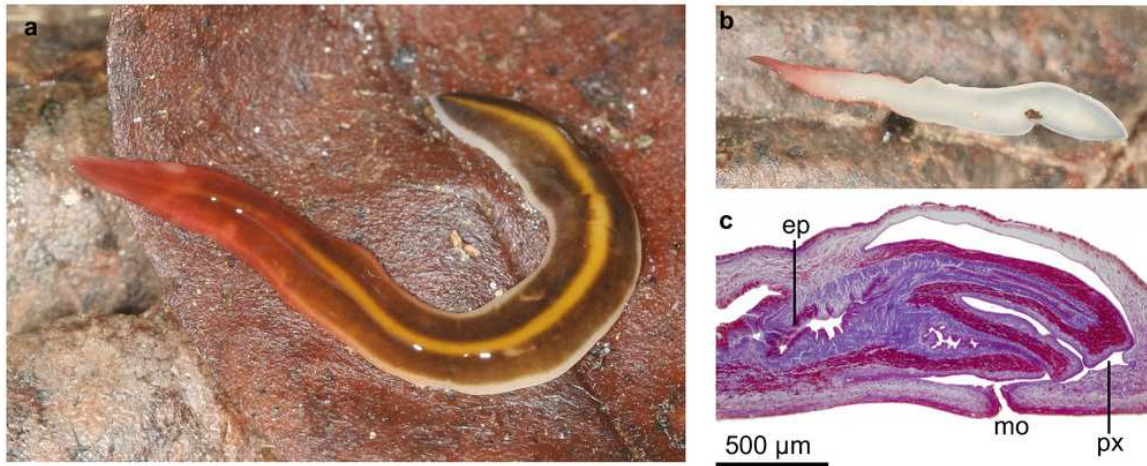


# Figure 13

*Cratera imbiri* ~~sp. n.~~ morphological features.

*Cratera imbiri* ~~sp. n.~~ Holotype. (A) diagrammatic representation of the copulatory apparatus from sagittal sections. (B): photomicrograph of a sagittal section of copulatory apparatus. (C): photomicrograph of a sagittal section of male atrium. (D): photomicrograph of a horizontal section of ovary.



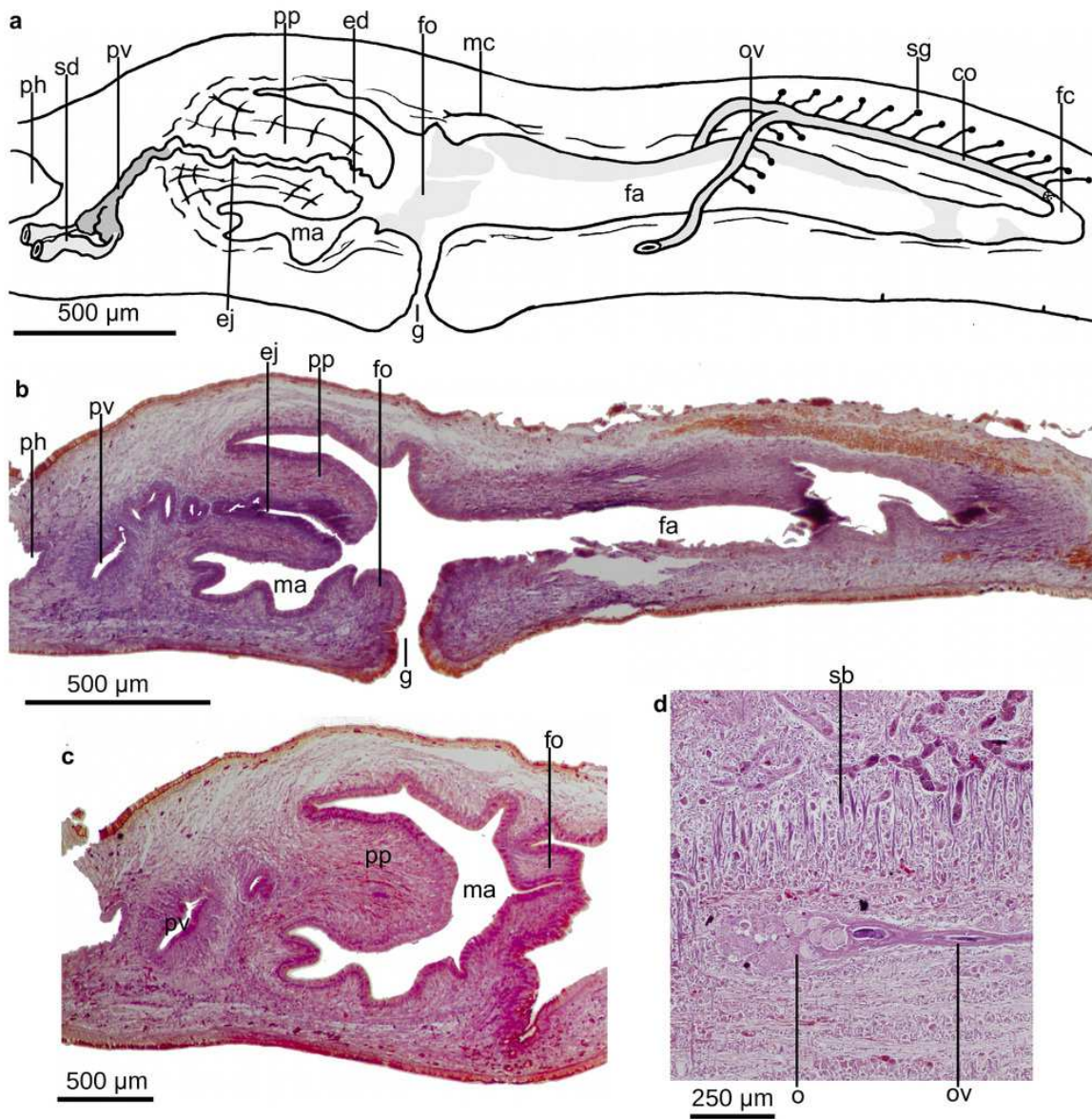


# Figure 14

*Cratera paraitinga* ~~sp. n.~~ morphological features.

*Cratera paraitinga* ~~sp. n.~~ (A): Dorsal view of living holotype. (B): Dorsal view of living paratype. (C): Ventral view of living paratype. Scales not available.





# Figure 15

*Cratera paraitinga* ~~sp. n.~~ morphological characters.

*Cratera paraitinga* ~~sp. n.~~ (A): photomicrograph of a transverse section of pre-pharyngeal region of paratype. (B): photomicrograph of a sagittal section of pharynx of holotype. (C): diagrammatic representation of the copulatory apparatus of holotype from sagittal sections.

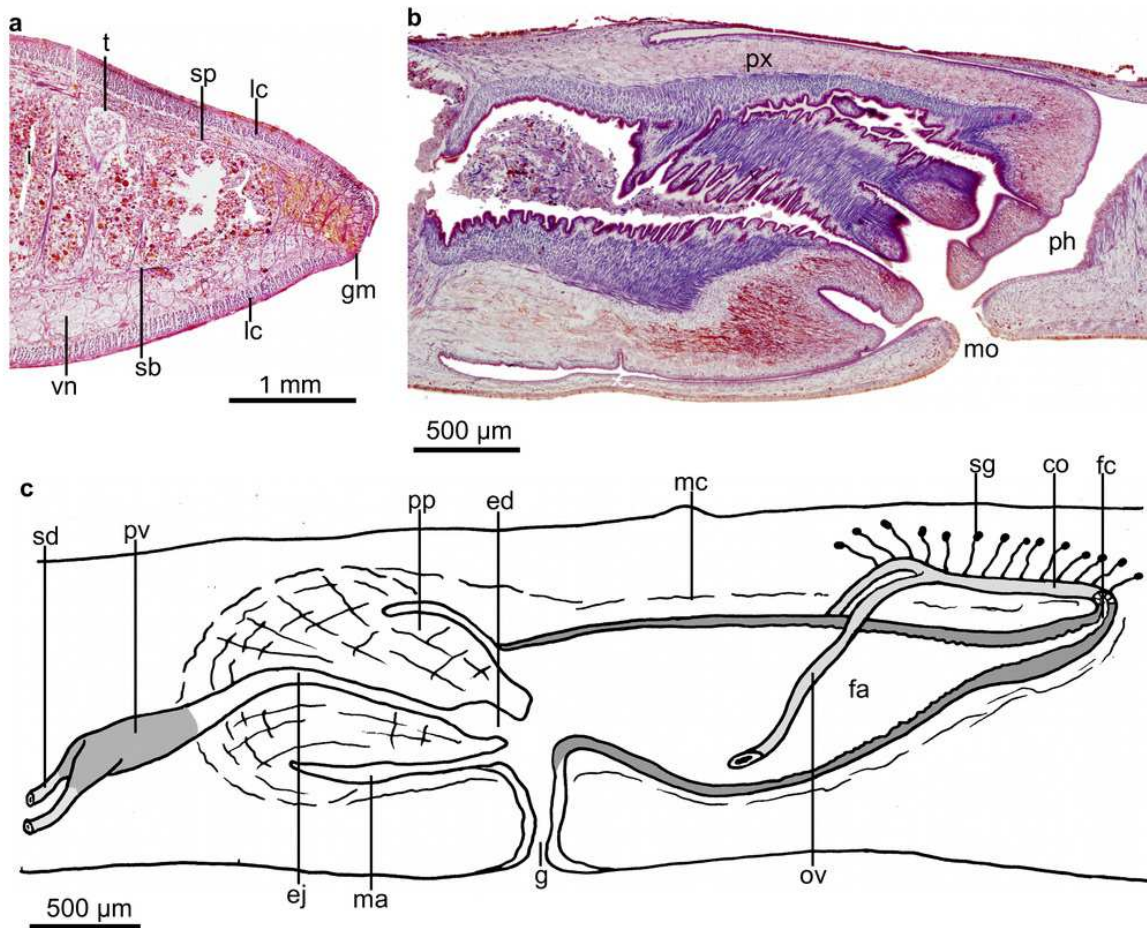


# Figure 16

*Cratera paraitinga* ~~sp. n.~~ morphological features.

*Cratera paraitinga* ~~sp. n.~~ Photomicrographs of sagittal sections. (A): sagittal section of copulatory apparatus of holotype. (B): Copulatory apparatus of paratype, incompletely mature. (C): Posterior region of female atrium of holotype.



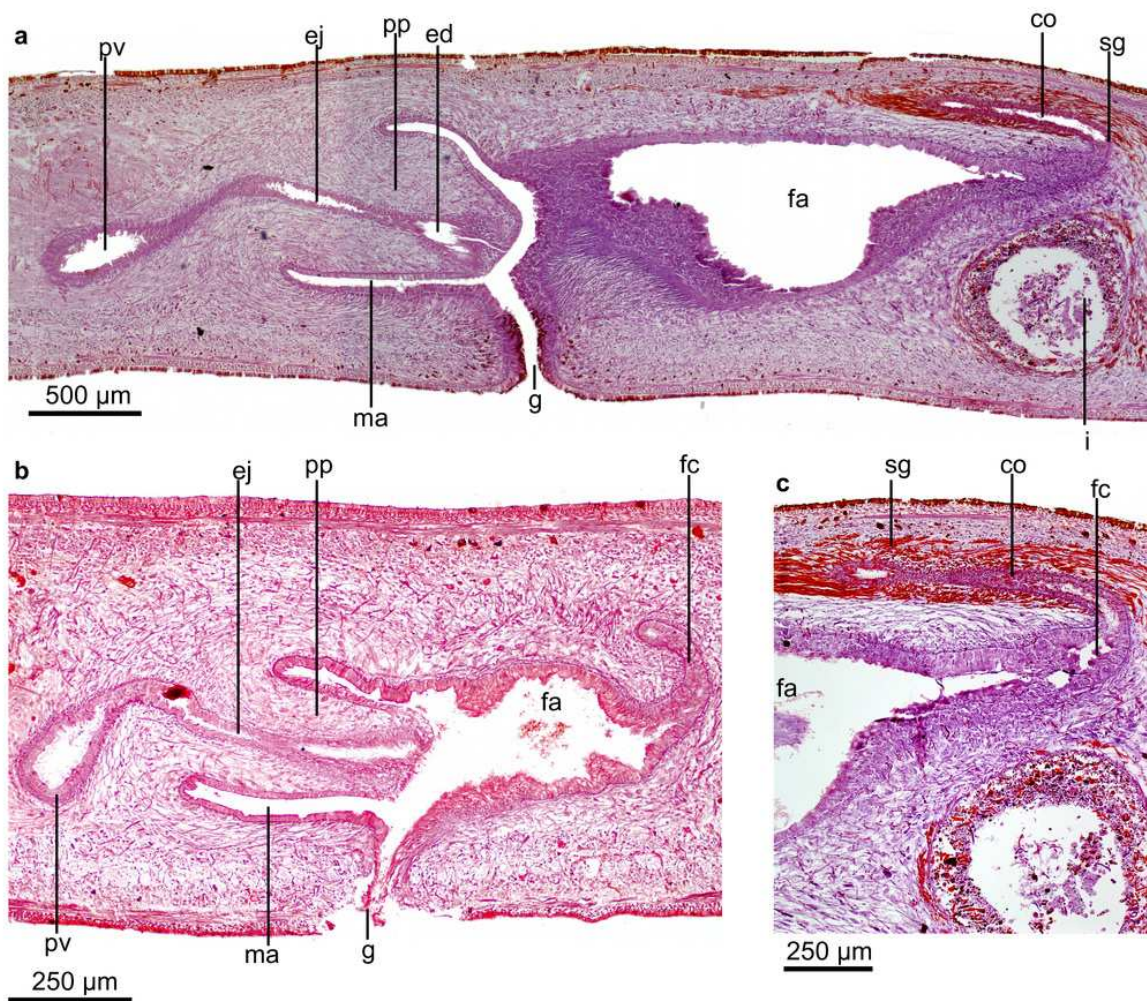


# **Table 1**(on next page)

List of *Cratera* samples used in this study with sampling locality, molecular code, voucher code and GenBank Accession numbers.

~~List of *Cratera* samples used in this study with sampling locality, molecular code, voucher code and GenBank Accession numbers.~~

1 **Table 1.** List of *Cratera* samples used in this study with sampling locality, molecular code, voucher code and GenBank Accession numbers.

Species	Sampling locality	Molecular code	Museum Code	GenBank Accession number					
				Cox1	Nd4Cox1	18S	28S	EF	Tnuc813
<i>Cratera arucuia</i>	P.N. Intervalles / SP	F2783	MZUSP <sup>a</sup> PL 1048	KC608281 <sup>c</sup>	MT468629*	KC608513	KC608396	KC614508	MT468607
<i>Cratera crioula</i>	P.E. Serra da Cantareira / SP	F2960	MZUSP PL 471	MT437776*	-	-	-	-	-
	P.N. Bocaina / SP	F2989	MZUSP PL 0459	KU564215	-	-	-	-	-
	P.E. Serra da Cantareira / SP	F3709	MZUSP PL 1078	KC608323	-	KC608557	KC608440	KC614543	MT468615
		F3715	MZUSP PL 1079	KC608324	-	KC608558	KC608441	KC614544	MT468616
<i>Cratera cuarassu</i>	P.E. do Desengano / RJ	F2189	MZUSP PL 348	MT437766*	MT468626*	KC608510	KC608393	KC614505	MT468603
		F2191	MZUSP PL 349	MT437767*	MT468627*	MT441688*	MT441711*	MT468580*	MT468604
		F2192	MZUSP PL 350	MT437768*	-	MT441689*	MT441712*	MT468581*	MT468605
		F2193	MZUSP PL 351	MT437769*	MT468628*	MT441690*	MT441713*	MT468582*	MT468606
		F4006	MZUSP PL 805	MT437777*	-	-	-	-	-
		F4014	MZUSP PL 806	MT437778*	-	-	-	-	-
	P.E. do Desengano / RJ	F4017	MZUSP PL 807	MT437779*	-	-	-	-	-
		F4041	MZUSP PL 808	MT437780*	-	-	-	-	-
<i>Cratera imbiru</i> sp. nov.	P.E. Campos de Jordão / SP	F5512	MZUSP PL 2155	MT437782*	-	MT441697*	MT441720*	MT468589*	MT468618
<i>Cratera ochra</i>			MZU PL.00192	KT250624 <sup>c</sup>	-	-	-	-	-
			MZU PL.00191	KT250623	-	-	-	-	-
			MZU PL. 1564	KT250622	-	-	-	-	-
<i>Cratera paraitinga</i> sp. nov.	Estação Bio. Boracéia /SP	F5745	MZUSP PL 2156	MT437783* <sup>c</sup>	MT468634*	MT441698*	MT441721*	MT468590*	MT468619
		F5769	MZUSP PL 2157	MT437784* <sup>c</sup>	MT468635*	MT441699*	MT441722*	MT468591*	MT468620

<i>Cratera picuia</i>	P.N. Saint Hilaire / PR	F1613	MZUSP PL 1008	KC608261	-	KC608493	KC608376	KC614491	MT468598
<i>Cratera piguaiaboja</i> sp. nov.	P.N. Bocaina / SP	F2828	MZUSP PL 458	MT437773*	-	MT441693*	MT441716*	MT468585*	-
Species	Sampling locality	Molecular code	Museum Code	Cox1	Nd4Cox1	18S	28S	EF	Tnuc813
<i>Cratera piguaiaboja</i> sp. nov.	P.N. Bocaina / SP	F2829	MZUSP PL 459	MT437774*	-	MT441694*	MT441717*	MT468586*	-
<i>Cratera piguaiassu</i> sp. nov.	P.N. Bocaina / SP	F2025	MZUSP PL 2146	MT437763*	-	MT441685*	MT441708*	MT468577*	MT468599
		F2807	MZUSP PL 1050	KC608284	-	KC608516	KC608399	KC614510	MT468609
		F2821	MZUSP PL 1052	KC608287	-	KC608519	KC608402	KC614513	MT468611
		F2825	MZUSP PL 2150	MT437772*	MT468631*	MT441692*	MT441715*	MT468584*	MT468612
		F2834	MZUSP PL 2151	MT437775*	MT468632*	MT441695*	MT441718*	MT468587*	MT468613
<i>Cratera piguaiatui</i> sp. nov.	P.N. Bocaina / SP	F2031	MZUSP PL 1014	KC608268 <sup>c</sup>	MT468625*	KC608500	KC608383	KC614497	MT468600
		F2040	MZUSP PL 2147	MT437764* <sup>c</sup>	-	MT441686*	MT441709 *	MT468578*	MT468601
		F2054	MZUSP PL 2148	MT437765*	-	MT441687*	MT441710 *	MT468579*	MT468602
		F2798	MZUSP PL 2149	MT437770* <sup>c</sup>	-	MT441691*	MT441714*	MT468583*	MT468608
		F2809	MZUSP PL 1051	MT437771* <sup>c</sup>	MT468630*	KC608517	KC608400	KC614511	MT468610
	P.N. Itatiaia / RJ	F5178	MZUSP PL 2154	MT437781*	MT468633*	MT441696*	MT441719*	MT468588*	MT468617
<i>Cratera pseudovaginuloides</i>	P.N. Órgãos / RJ	F1244	MZUSP PL 670	KC608251	MT468622*	KC608483	KC608366	KC614482	MT468593
		F1245	MZUSP PL 671	KC608252	-	KC608484	KC608367	KC614483	MT468594
<i>Cratera tamoia</i>	P.N. Órgãos / RJ	F1139	MZUSP PL 665	KC608246	MT468621*	KC608478	KC608361	KC614478	MT468592
		F1336	MZUSP PL 672	KC608254	MT468623*	KC608486	KC608369	KC614484	MT468595
<b>Outgroup</b>									



<i>Obama anthropophila</i>	P.N. Itajaí / SC	F1399	MZUSP PL 1007	KC608256	MT468624*	KC608488	KC608371	KC614486	MT468596
<i>Obama ladislavii</i>		F1418	MZUSP PL 681	KC608258	-	KC608490	KC608373	KC614488	MT468597
<i>Obama josefi</i>	FLONA <sup>b</sup>	F3403	MZUSP PL 1075	KC608318	-	KC608552	KC608435	KC614538	MT468614

<sup>a</sup> Vouchers are deposited in the Museu de Zoologia da Universidade de São Paulo (MZUSP)

<sup>b</sup> Floresta Nacional de São Francisco de Paula

<sup>c</sup> Short fragment

\*This study